UDC 66.021.1:532.5,661.15,661.15 66.021.1:532.5
No of state registration 0120U100476
Inv. No

Ministry of Education and Science of Ukraine
Sumy State University
40007, Sumy, R.-Korsakova str., 2;
phone. (0542) 33-41-08/33-40-49

APPROVED
Vise-rector for scientific work
D.Sc. (physics and mathematics),
professor

_____ A.M. Chornous

REPORT
ON RESEARCH WORK

Technological bases of multistage convective drying in small-sized devices with utilization and heat recovery units

EXPERIMENTAL STUDIES OF THE HYDRODYNAMICS OF FLOW MOTION AND HEAT AND MASS TRANSFER PROCESSES IN DRYING UNITS USING GRAVITY SHELF DRYERS

(intermediate)

Manager of research work
Ph.D. (technical sciences), N.O. Artyukhova

2021

The manuscript was complete on November 18, 2021.

The results of this work were considered by the Scientific Council, Minutes from 2020.11.25 No. 5

ABSTRACT

Report on research work: 100 p., 131 figures, 6 tables, 153 references.

DIRECTIONAL MOTION OF THE FLUIDIZED BED, DRYING, MULTISTAGE DRYER, PERFORATET SHELF, HYDRODYNAMICS, KINETICS

The following new *scientific results* were obtained during the research:

1. The fields of gas flow velocity in the working space of the gravity shelf dryer are obtained. The limits of existence of each of the hydrodynamic modes of operation of the device are shown experimentally.

2. Temperature-humidity characteristics of interacting flows and values of efficiency of stages of the dryer depending on the design of shelves and the organization of movement of the drying agent are received. It is shown that the most significant influence on the change of temperature and humidity characteristics has the time of the material on the step, which is due to the angle of the shelves and their length.

3. Under different conditions of the experiment, the range of efficiencies of individual stages of the dryer in the range of 0.12-0.47 was determined. The amount of moisture removed from the material may be from 4 to 8% of the mass. The initial value of the moisture content of the dispersed material of 13% of the mass.

4. It is shown that by changing the design of the shelf and the organization of the drying agent (in particular, in the case of its bypass), it is possible to control the drying time of the material and the efficiency of the steps of the dryer. The angle of the shelf can have a minimum value that corresponds to the angle of the natural slope of the material.

The practical significance of the obtained results.

Based on the received experimental data, the technique of engineering calculation of shelf dryers with vertical sectioning of working space is improved. An improved design of a multi-stage shelf dryer is proposed, making it possible to separate fine particles on the first perforated contact shelf. The experimental results obtained in this work will be used in the future to perform economic contract work on the provision of information and

analytical services for selecting optimal drying schemes and services for the development of design documentation for the design of multi-stage dryers.

Together with representatives of Alexander Dubcek University of Trencin (Slovakia), as well as the University of Pardubice and J.E. Purkyne University in Usti nad Labem (Czech Republic) based on theoretical and experimental data, continues to develop a software package for calculating the technological parameters of the gravity shelf dryer and its design dimensions.

TABLE OF CONTENTS

INTRODUCTION

Report section "Introduction" is prepared in according to data [1,2].

Today the granular mineral fertilizers and bulk granular products are produced using several typical technological processing schemes. When developing technical plans for producing mineral fertilizers, developers and constructors face the difficulties in selecting the necessary equipment for the operating production departments, namely, for the granulation and enlargement of granules, their drying, cooling, and pneumatic separation.

The most effective units to implement the above purposes are fluidized bed devices. One should mention that despite effective processes in the fluidized bed, the heat-mass transfer ends at a low layer height, nearby the grid zone. In this case, most energy in the gas flow is taken for the hydrodynamic stabilization of the fluidized bed, the height of which reaches 0.2–0.5 m. It increases energy consumption and abrasion of particles, causing the necessity to install energy-intensive and metal-intensive dust cleaning systems.

Thus, scientific research in the field of dispersed system processes intensification should be oriented primarily to the development of energy-saving fluidized-bed devices with a new organization of gas-dispersed flows, in which minimal costs for the process and dust cleaning provide an adequate efficiency. Multistage shelf devices implement these tasks. In shelf devices, active aerodynamic regimes of solid particles weighing are implemented, and the conditions for their creation, unlike typical fluidized bed devices, can be easily changed over a wide range of gas flow velocities without fundamental changes in the construction.

A comprehensive assessment of the quality of the drying process is determined not only by the amount of removed moisture and the provision of the material's necessary physical and chemical properties. It is also necessary to consider the energy costs of the drying process, the simplicity or complexity of the design of the dryer, the possibility of ensuring optimal technological parameters of the process, the possibility of utilizing and recovering heat and moisture, etc. Thus, the drying method's choice and the dryer design

is a multifactorial theoretical and experimental study with elements of optimization for a given objective function.

The convective drying process is one of the most common in the technology of dehydration of dispersed materials. Despite the indisputable advantages, the convective drying process as technology and dryers as "executors" of this technology require improvement. In particular, in the process of convective drying, it is necessary to solve the following problems:

- ensuring the minimum contact time of the drying agent with dispersed material;

- ensuring the maximum driving force of the drying process in the working space of the apparatus;

It should also be noted that it is not always possible to ensure the required residence time of the material in a convective dryer with a classical fluidized bed due to intensive mixing of the material and different moisture gradients in different parts of the apparatus.

In addition, in such devices, it is difficult to uniform contact of the dispersed material and the drying agent in a wide range of phase loads (flow ratio). This complicates the process of dewatering thermolabile dispersed materials, such as cereals. Significant costs for heating and pumping the drying agent are also disadvantages of the considered devices.

Carrying out this process using an active hydrodynamic regime, which provides an increase in the relative velocity of the interacting phases, contributes to the process's intensification without reducing the apparatus's economic efficiency. The advantages of the active hydrodynamic regime also include:

- hydrodynamic stability of the process;

- providing a developed surface of the interaction of contacting phases;

- reducing the energy consumption of the process and the metal consumption of the apparatus.

One of the methods of convective drying is the contact of a material with a heat carrier in a stationary, suspended, or semi-suspended state. Currently, convective dryers are most often used, in which the material is dried in a suspended (fluidized) state.

The main advantages of multi-stage fluidized bed dryers are:

- multifunctionality of the apparatus - the ability to simultaneously carry out the process of drying, classification and separation of particles;

- creation of a countercurrent mode of movement of interacting flows;

- the organization of a differentiated mode of dehydration of dispersed material - the creation of different conditions for drying the material at each stage, depending on its temperature and humidity characteristics;

- the ability to control the residence time of particles at each stage of the apparatus and in the apparatus as a whole.

Improvement of devices with a fluidized bed for mass transfer in the "gas-solid" system is possible by organizing the mutual movement of flows with repeated use of the fluidizing agent, for example, when sectioning the dryer by installing shelf contacts along with its height. In shelf units, the processes of pneumatic classification, dedusting, cooling, granulation, etc., are implemented. Such devices are not widely used in drying processes. Due to the multiple contact of the dispersed material with the drying agent, it becomes possible to reduce material and energy costs for the process significantly.

In the proposed apparatus for the implementation of intensive drying methods, it is assumed that the internal space is sectioned by establishing a cascade of perforated shelves at a certain angle, creating conditions for the gravitational movement of material along the shelves and its transfer from one shelf to another. On each of the shelves in this design, effective mixing inherent in the suspended bed is created while maintaining the advantages of an organized countercurrent mode.

The presence of inclined perforated shelves in the working space of the shelf dryer reduces its free cross-sectional area. This design solution causes a local increase in the velocity and degree of turbulence of the flow of the drying agent, as well as changes in the nature of the velocity distribution around the shelf.

The indicators of heat and mass transfer processes in the suspended layer are essentially determined by the hydrodynamic indicators of the movement of continuous (gas) and dispersed (solid) flows. The efficiency of the apparatus of the suspended layer

largely depends on the flow field of the gas flow, the distribution of which over the working space of the apparatus affects the profile of temperatures and concentrations of the granular material.

Justification of the possibility of using multistage devices with vertical sectioning of the working space and determines the relevance of the presented article.

The object of research is gravitational shelf dryers for the dehydration of dispersed materials.

The subject of research is the hydrodynamics of flow within the cascade of shelf contacts.

1 MULTISTAGE SHELF DEVICES WITH FLUIDIZED BED FOR HEAT-MASS TRANSFER PROCESSES: EXPERIMENTAL STUDIES AND PRACTICAL IMPLEMENTATION

Today the granular mineral fertilizers and bulk granular products are produced using several typical technological processing schemes. When developing technical plans for producing mineral fertilizers, developers and constructors face the difficulties in selecting the necessary equipment for the operating production departments, namely, for the granulation and enlargement of granules, their drying, cooling, and pneumatic separation.

The most effective units to implement the above purposes are fluidized bed devices. One should mention that despite effective processes in the fluidized bed, the heat-mass transfer ends at a low layer height, nearby the grid zone. In this case, most energy in the gas flow is taken for the hydrodynamic stabilization of the fluidized bed, the height of which reaches 0.2–0.5 m. It increases energy consumption and abrasion of particles, causing the necessity to install energy-intensive and metal-intensive dust cleaning systems.

Thus, scientific research in the field of dispersed system processes intensification should be oriented primarily to the development of energy-saving fluidized-bed devices with a new organization of gas-dispersed flows, in which minimal costs for the process and dust cleaning provide an adequate efficiency. Multistage shelf devices implement these tasks. In shelf devices, active aerodynamic regimes of solid particles weighing are implemented, and the conditions for their creation, unlike typical fluidized bed devices, can be easily changed over a wide range of gas flow velocities without fundamental changes in the construction.

Devices with various construction are used for granulation in a fluidized bed. The shape of the unit defines the hydrodynamic features of the process. In the conical-cylindrical part of the device, fluidization is uniform over the entire section in a more than 300 mm height bed [1,2] that increases the energy cost for weighing a high bed. There is

a local spouting zone with an additional supply of gas flow in the center of the gas distribution grid [3]. This approach increases the heat-mass transfer process efficiency. However, it requires a separate supply of gas flow into the holes of the gas distribution grid and the nozzle in its center. In some fluidized bed granulators, a special spraying mode of the melt by the nozzle is formed [4,5], or a fluidization jet-pulsating mode is created [6].

The fluidized bed enables to intensify the contact of the phases between the drying agent and the surface of the particles, which are convectively dried [7]. Moreover, both traditional drying technologies in a fluidized bed and special drying using acoustic fields, microwave heating, vibration, or special mixing methods are implemented. The microwave heating of ceramic microspheres in a fluidized bed made it possible to control the drying kinetics without significant agglomeration of the dried particles [8]. The vibrational oscillations overlaid on a fluidized bed of solid particles are mostly applied in the fluidization method. A positive effect has been proved in the intensification of phase contact in a vibrating fluidized bed, in comparison with a stationary layer, optimal features are selected [9,10]. It is indicated that gas-vibro-fluidization usually has higher circulation velocities compared to conventional gas-fluidization [11]. The vertical oscillations overlaying the vibration layer shows that vibration can help fluidize particles, and the axial and radial distribution of holes in a layer with vibration is more uniform than without it [12].

Fluidized bed devices in the mineral fertilizers producing technology are mostly known as coolers for granular materials [13–15]. Although heat exchange processes in a fluidized bed are efficient enough, these devices are characterized by increased specific consumption of cooling air.

The authors of [16] proposed to use a vertical device with a fluidized bed of granules on vibrating blades for cooling granules. It is indicated that synchronous oscillations of the blade and the fluidization regime affect the final temperature and humidity of the granules during the cooling process. However, the complexity and

operational unreliability of the construction is confirmed by the presence of cushioning springs and vibration devices.

In fluidized bed units, during fluidization, small particles are separated with the ascending gas flow. Their number is identified either by hydrodynamic factors (gas flow velocity) and layer height [17] or by granulometric composition and physical properties of the particles in the initial product [18,19]. The positive effect of vibrational oscillations on the separation process of small particles from the fluidized bed is noted [20,21].

The constructive parameters also identify the fluidization quality. Thus, in [22], the motion of particles in a stable turbulence regime of a fluidized bed was studied when the air distribution blades were installed at different angles, which led to stable layer fluidization of particles of various sizes and shapes. In the work [23], a system for the more uniform supply of the product to a fluidized bed was studied, and in [24] the authors indicated that hydrodynamics and heat transfer can be significantly improved due to the internal circulation of solid particles using two gas distributors.

The complex hydrodynamics of the fluidized bed by a gas flow is described by disordered mixing of solid particles and the formation of gas bubbles, that is confirmed in [25–29]. The effect on the fluid dynamics of a fluidized bed of various parameters was studied: gas injection time into the bed, gas flow velocity and bubbling regime [25], bubble dynamics during nonspherical particles fluidization [26], continuous injection of the central air jet into the bed [27], and features of the pseudo-two-dimensional two-zone gas–solid fluidized bed [28], from the features of solid particles and gas bubbles [29]. Researchers also paid attention to the study of the interphase heat transfer intensity between particles and the gas flow [30] and heat transfer to heat exchange surfaces located in the layer [31–34]. The research in [31] studied the effect on the heat transfer of the gas flow uneven distribution, which led to the heat transfer intensification due to the higher packet updating frequency. The research in [32] considered the influence of the rate of contact renewal between solid particles and a vertical heat tube placed in a fluidized bed. In [33], the influence of the bubble frequency and gas retention on heat transfer with vertical tubes dipped into a fluidized bed was studied. Since the coefficients

of heat transfer between particles and heat transfer surfaces are higher in the center of the layer than at its periphery, it is proposed in [34] to use a gas distributor with an inhomogeneous nozzle array to overcome the unevenly distributed heat transfer.

Thus, the above review of scientific articles showed that researchers direct their efforts to a detailed study of the hydrodynamic and structural features of the fluidized bed to increase the operating efficiency of the device. However, at the same time, one of the significant drawbacks of fluidized beds consists of rather high energy costs to weigh a significant amount of material on a gas distribution grid (more than 1–2 m3 of gas/kg of product). The separation of small particles of less than 500 μm in size from the fluidized bed leads to the formation of large volumes of dusty exhaust gas with a low dust concentration in it. Purification of such gases from dust requires powerful gas cleaning systems.

The fluidized bed devices for organizing the motion of gas-dispersed flows are between shaft-type devices (with particles of material falling downward and moving countercurrent of gas) [35,36] and pneumatic transportation devices (with direct ascending flow motion) [37]. Both types have disadvantages—insignificant contact of phases and, accordingly, low heat transfer coefficients between particles and gas flow, as well as the short residence time of particles in a flow. Therefore, such devices are not so effective and are very high-priced.

One of the solutions that allow stabilizing the operation of a fluidized bed apparatus is the swirling of flows, which has found application, for example, in the granulation devices [38]. The data of theoretical [39] and computer [40] modeling of the operation of such devices as applied to the production of porous ammonium nitrate [41] is confirmed by the successful testing of product samples [42].

The authors of this article have chosen another way to improve the fluid dynamics of the fluidized beds—namely, a method to weigh solid particles on a gas distribution grid. The gas distribution grid (shelf) is installed in a vertical channel at an angle of 25–45° to the horizon forming the outloading space between the end of the shelf and the channel wall. There can be several shelves throughout the height of the device. This

feature enables to create various gas-dispersed flow modes in shelf units, in which not only the basic features of the flow are quantitatively changed (concentration of solid particles in the gas flow, velocities, heat-mass transfer coefficients), but there are qualitative changes in flow structure, phase motion mechanism, and heat-mass transfer conditions under certain critical conditions. Thanks to the various hydrodynamic modes of the solid particles transfer (from the gravitationally falling to the weighted layer), the shelf contact elements provide higher efficiency of heat-mass transfer [43,44] and separation [45] processes with a lower gas flow rate and hydraulic resistance than typical fluidized bed devices do.

High efficiency, lower capital and operating costs, small dimensions and hydraulic resistance, higher specific productivity of shelf devices in comparison with typical units of a weighted layer, make the first up-and-coming devices for being used in various industries.

Experimental research was carried out in the device with a cross-section of 50 × 100 mm and a height of up to 1 m with a separation space (Figure 1).

Shelf contact elements differ from gas distribution grids of fluidized-bed devices and wedge-shaped elements plates primarily due to the presence of outloading space between the end of the shelf and the wall in the unit (Figure 1). The width of the outloading space is expressed by the ratio Lcl/Ldev, where Lcl is the distance between the end of the shelf and the wall of the device, and Ldev is the length of the side section of the device. It is possible to influence the gas flow distribution between the outloading space and the holes of the shelf, as well as on the ascending flow velocities in the separation space and the solid phase, moving along the shelf, by varying the Lcl/Ldev ratio, the perforation degree of the shelf ψ. The tilt angle of the shelf γ to a lesser extent affects the velocities profile of the gas flows over the outloading space and the holes of the shelf. The optimal tilt angle of the shelves is $\gamma = 25°$ to the horizontal plane (Figure 2). The material particles lay on the surface of the shelf at a smaller angle. The particles quickly roll down to the outloading space and do not form a weighted layer above the shelf at a larger angle. The distance between the end of the upper shelf and the beginning

of the lower shelf Ls is determined by the ratio between this distance to the length of the lateral part of the section in the device—Ls/Ldev. If Ls/Ldev < 0.5, the gas flow velocity in the outloading space increases. As a result, the free flow of material particles is impeded through the outloading space to the lower shelf. As the distance Ls increases, the gas flow velocity in the outloading space naturally decreases. When Ls = Ldev the flow rate is constant. Therefore, we take $0.5 < Ls/Ldev \leq 1$ in the construction of the device.

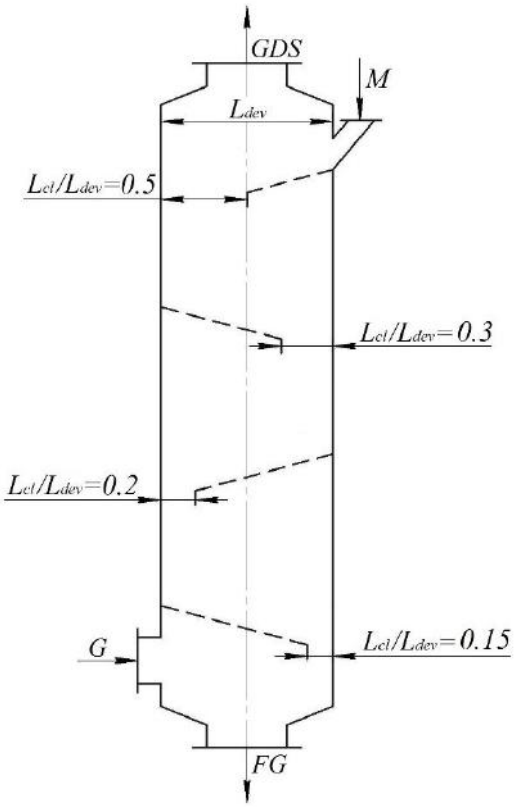

Figure 1 – Multistage shelf device circuit: M—raw material; G—gas; GDS—gas-dispersed substance; FG—finished granules

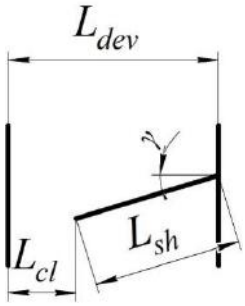

Figure 2 – The basic elements of the shelf device construction

A polydisperse granular superphosphate mixture in the form of a 0.1–5 mm granule with a shape factor of 0.85 was used in the studies. The sieve analysis using wire sieves with aperture sizes (the size of the square hole side) 0.5, 1.0, 1.6, and 2.5 mm defined the granulometric composition of the polydisperse mixture. The sieves were folded in a vertical block with decreasing hole sizes from top to bottom and installed on a vibrating table with a control unit. Sieve analysis was carried out for 15–20 min, corresponding to the measurement accuracy [46]. Several samples were analyzed according to the methodology to assess the accuracy of the measurement [47]. The deviation of the results for each sample did not exceed 1.5–2.0%. The results of the sieve analysis of the initial polydisperse mixture are as follows: +2.5 mm—10%; 2.5 + 1.6 mm—25%; 1.6 + 1 mm—25%; 1 + 0.5 mm—20%; 0.5 mm—20%. According to the reference data, the true and bulk density of superphosphate granules obtained by the nodulizing method in a drum granulator was 2250 kg/m3 and 1100–1200 kg/m3 [48].

The laboratory unit consisted of a device equipped with a loading hopper with a belt feeder and an unloading hopper, a centrifugal cyclone to capture fine fractions with an unloading hopper, a high-pressure fan for pumping air through the device, and a cyclone. The walls in the device from the front side were transparent for visual observation and filming.

The initial mixture of the granulated superphosphate with amount of 3 kg was weighed on an electronic scale with an accuracy of 0.1 g. The mixture was heated to 90–95 °C in the loading hopper with electric heating elements (it corresponds to the

temperature at the outlet of the drum granulator dryer [49]) and fed by the belt feeder into the device on the upper shelf. The moisture content of the granules was less than 1 wt% at this temperature, not affecting the heat transfer process [50]. The specific productivity of the raw material was 6–10 kg/(m2·s). Air was sucked through the device by a high-pressure fan. The air flow was regulated and measured by a calibrated collector with a control valve. The air temperature at the inlet to the device was equal to the temperature in the laboratory: in summer conditions—22–27 °C; in winter conditions—18–22 °C. The material cooled to a temperature of 40–45 °C, was accumulated in the unloading hopper and unloaded at the end of the experiment. A small fraction of the material was trapped in the cyclone by the ascending air flow. When the device operated in a stationary mode (it was installed 15–20 s after turning on the feeder), 5–6 were selected from the unloading hopper and after the cyclone. The unloading hoppers were doubled to eliminate air leaks during material sampling. Spring-loaded valves were installed in the lower hopper. Then, the samples were weighed on an electronic scale with an accuracy of 0.1 g. For sieve analysis, the arithmetic mean value was taken from the weights of the selected samples. Several samples taken during repeated experiments under the same conditions were analyzed to assess the accuracy of the performed measurements. The deviation of the measurement results for each fraction between the selected samples was 1.5–2.0%. There were six experiments to eliminate the influence of random factors on the reliability of the measurement results.

The research regarding the features of one- and two-phase flows motion hydrodynamics in a shelf device was carried out with gas flow velocities of 1–5 m/s. A semiconducting thermoanemometer with an accuracy of 0.001 m/s measured the gas flow velocities in the workspace of the device. The measuring sensor was installed in the unloading space and the area above the shelf every 10 mm along the horizontal line. The measuring sensors were moved in height every 40 mm. There were four horizontal measurement lines above the shelf. The position of the thermoanemometer sensor was determined by the Xdev/Ldev ratio, where Xdev is the current distance from the initial plane (the left wall of the device) along the section length Ldev of the device.

An alcohol U-shaped manometer measured the pressure difference of the device. One tube of the manometer was connected to a point of the body under the lower shelf, and the second—at the gas outlet after the upper shelf. The measurement error when setting two levels (on each tube) was ±2 mm at an ambient temperature of 20 ± 5 °C.

One used filming under stroboscopic illumination at a frequency of 32 frames per second through the transparent walls of the device for establishing the mechanism and peculiarities of the gas-dispersed flow motion.

The research on the heat transfer peculiarities between the solid phase and the gas flow was carried out by cooling the superphosphate granules with an air flow. The temperature regime in the workspace of the device was controlled by thermocouples "Chromel-Copel" with open junctions through a self-recording potentiometer with an accuracy of 0.5 °C.

The thermocouple sensor was a protective metal case like a tube with a diameter of 1 mm and 60 mm long. There was a junction of interconnected chrome and copel thermoelectrodes 0.1 mm in diameter at the end of the tube. The heat capacity of this junction is negligible. It enables to perform measurements under conditions of continuously changing temperatures. Temperature sensors were installed at the following points: in the outside air supply pipe—to the device, in the loading hopper and unloading hoppers—after the device and the cyclone, in the separation space—at the outlet of the gas-dispersed flow from the device. The weighted layer temperature on the lower shelf was measured by placing three sensors along the entire length of the shelf at the height of up to 5–8 mm, one in the unloading space area and two at the gas flow outlet from the weighted layer.

The heat transfer coefficient was calculated from the basic equation of heat transfer, while the total surface area of the particles was estimated per unit volume of the layer. This approach is also confirmed in [51,52]. The velocities of solid particles in the layer are small compared to the gas flow rate. The ratio between the gas velocity in the free section of the device and the gas velocity between the particles in the layer varies over

the section and height of the device. Therefore, it is advisable to consider the gas flow rate in the free section of the device when determining the Reynolds criterion.

As a criterion for assessing the cooling degree of the product in the cooler, a cooling coefficient was used, which is the ratio of the actually removed heat to the amount of heat that is removed when the material is completely cooled to the initial temperature of the cooling air:

$$K_{cool} = \frac{Q_{act}}{Q_{ful}} = \frac{t_{gi} - t_{gf}}{t_{gi} - t_{ai}}, \quad (1)$$

where t_{gi}, t_{gf}, t_{ai}—respectively, the initial, final temperature of the granules, and the initial temperature of the cooling air, °C.

The efficiency of small particles separation from the weighted layer was characterized by the small fraction extraction degree into the ablation $\varepsilon_м$, representing the ratio of the small fraction size in the ablation to its amount in the raw material.

The total aerodynamic resistance ΔP is defined as a set of resistances of the degrees in the shelf device (pressure loss on the shelf) Δp_i [53]:

$$\Delta P = \sum_{i=1}^{n} \Delta p_i \quad (2)$$

The aerodynamic resistance of each shelf contact depends on the nature of the gas flow interaction with the shelves, installed at a certain angle, the shelf perforation degree ψ, the dispersed material amount in the inter-shelf space, characterized by the layer porosity ε or the concentration of the solid particles in the workspace of the device β. One should note that the specified pressure drop in the holes will decrease along the shelf. Therefore, the efficiency of the perforation holes with the same diameter will also decrease approaching the outloading space.

The pressure loss for elementary jet moving along a perforated shelf can be considered as the sum of the losses along the shelf length with the current coordinate X and local loss through the perforation holes:

$$\Delta p_i = const = \lambda \cdot \frac{X}{d_e} \cdot \frac{\rho_{gas} \cdot W_{gas}^2}{2} + \xi_{hol} \cdot \frac{\rho_{gas} \cdot W_{hol}^2}{2}, \quad (3)$$

where $\lambda \cdot \frac{X}{d_e} \cdot \frac{\rho_{gas} \cdot W_{gas}^2}{2} = \Delta p_l$ —pressure loss along the shelf length with current coordinate, Pa (where λ—friction coefficient);

d_e is the equivalent diameter of the shelf contact, m; $d_e = \frac{4L_{sh}B_{dev}}{2(L_{sh} + B_{dev})}$ [54];

L_{sh} is the shelf length, m; B_{dev} is the width of the device, m;

W_{gas} is the cross section velocity of the gas flow, m/s;

ρ_{gas}—gas flow density, kg/m^3;

$\xi_{hol} \cdot \frac{\rho_{gas} \cdot W_{hol}^2}{2} = \Delta p_{hol}$ —local loss in the perforation hole, Pa (where ξ_{hol} is the coefficient of the hole resistance);

W_{hol}—flow velocity in the perforation holes, m/s.

Thus, the total pressure loss between the control cross-sections consists of two components:

$$\Delta p_i = \Delta p_{hol} + \Delta p_l, \quad (4)$$

where

$$\Delta p_{hol} = \Delta p_i - \Delta p_l. \quad (5)$$

The nature of the gas flow jet lines along the shelf was experimentally confirmed [55]. It shows the parallel flow of two phenomena—the shelf bending and passing through its holes.

Air velocity in the perforation holes:

$$W_{hol} = \varphi \cdot \sqrt{\frac{\Delta p_{hol}}{\rho_{gas}}} = \varphi \cdot \sqrt{\frac{\Delta p_i - \Delta p_l}{\rho_{gas}}} = \varphi \cdot \sqrt{\frac{\Delta p_i - zX}{\rho_{gas}}}, \quad (6)$$

where φ is the velocity coefficient, which is 0.97–0.98 according to the experimental data [56];

z—specific pressure loss along the length, Pa/m.

The air flow loss through the holes of the shelf perforation is the following:

$$V_{sh} = \int_0^{L_{sh}} W_{hol} df_{sh} = \varphi \cdot B_{dev} \int_0^{L_{sh}} \psi \cdot \sqrt{\frac{\Delta p_i - zX}{\rho_{gas}}} dX, \quad (7)$$

where $df_{sh} = dX \cdot B_{sh}$;

ψ—degree of shelf perforation (free shelf cross-section);

f_{sh}—shelf area, m^2.

In the outloading space L_{cl} (Figure 2) the pressure drop Δp_{cl} will be minimal:

$$\Delta p_{cl} = \Delta p_i - zL_{sh}, \quad (8)$$

and the air flow loss is defined as

$$V_{cl} = \varphi \cdot L_{cl} \cdot B_{dev} \cdot \sqrt{\frac{\Delta p_i - zL_{sh}}{\rho_{gas}}} \cdot \quad (9)$$

Total air flow rate is $V_{sh} + V_{cl}$. We will define the total air flow rates by integrating the ascending velocity function along the length of the perforated shelf and taking the constant perforation degree:

$$V = B_{dev} \int_0^{L_{sh}} W_{hol} dX = \varphi \cdot \psi \cdot B_{dev} \int_0^{L_{sh}} \sqrt{\frac{\Delta p_i - zX}{\rho_{gas}}} dX \cdot \quad (10)$$

Substitution of the subintegral expression by a function $y = \Delta p_i - zX$, where $dy = -zdX$ enables to obtain the integration result within (0, L_{sh}):

$$V_{sh} = \frac{-B_{dev} \cdot \varphi \cdot \psi}{z \cdot \sqrt{\rho_{gas}}} \int_0^{L_{sh}} y dy = \frac{2 \cdot B_{dev} \cdot \varphi \cdot \psi}{3 \cdot z \cdot \sqrt{\rho_{gas}}} \cdot \left(\sqrt{\Delta p_i^{\,3}} - \sqrt{(\Delta p_i - z \cdot L_{sh})^3} \right) \cdot \quad (11)$$

The share of the flow through the outloading space is added to the balance equation of air flow rate along the cross-section of the shelf unit:

$$W_{gas} \cdot L_{dev} \cdot B_{dev} = V_{sh} + V_{cl} =$$
$$= \frac{2 \cdot \varphi \cdot \psi}{3 \cdot z \cdot \sqrt{\rho_{gas}}} \cdot B_{dev} \cdot \left(\sqrt{\Delta p_i^{\,3}} - \sqrt{(\Delta p_i - z \cdot L_{sh})^3} \right) + \varphi \cdot L_{cl} \cdot B_{dev} \cdot \sqrt{\frac{\Delta p_i - z \cdot L_{sh}}{\rho_{gas}}}, \quad (12)$$

where $W_{gas} \cdot L_{dev} \cdot B_{dev}$—total air flow rate in the device.

The analysis of Equation (11) allows to calculate the gas flow velocity above the perforated shelf with the free cross-sectional area $f_{cs} = \psi \cdot L_{sh} \cdot B_{dev}$:

$$W_{cr1} \cdot \psi \cdot L_{sh} \cdot B_{dev} = \frac{2 \cdot \varphi \cdot \psi}{3 \cdot z \cdot \sqrt{\rho_{gas}}} \cdot B_{dev} \cdot \left(\sqrt{\Delta p_i^{\,3}} - \sqrt{(\Delta p_i - z \cdot L_{sh})^3} \right) \cdot \quad (13)$$

This ratio defines the pressure loss Δp_i when installed in the workspace of one shelf device. It is possible to vary the constructive parameters of the shelf, namely its length and perforation degree. It is also possible to obtain profiles of the vertical velocities of the gas flow in the space above the shelf and the outloading space according to the algorithm below.

Comparing the total flow rates in the perforation holes to the flow rates calculated through the total area of the shelf $\left(W_{hol} \cdot \psi \cdot f_{sh} = \overline{W_{hol}} \cdot f_{sh} \right)$, one can find the average velocity

of the gas flow over the perforation holes in the vertical direction, taking into account Equation (6):

$$W_{gas} = \overline{W_{hol}} = \psi \cdot W_{hol} = \psi \cdot \varphi \cdot \sqrt{\frac{\Delta p_i - zX}{\rho_{gas}}} \cdot \quad (14)$$

An analysis of this expression showed, first, that the local velocity of the gas flow above the holes in the vertical direction decreases linearly depending on the shelf perforation degree ψ and nonlinearly in the X direction along the shelf length to the outloading space (Figure 3).

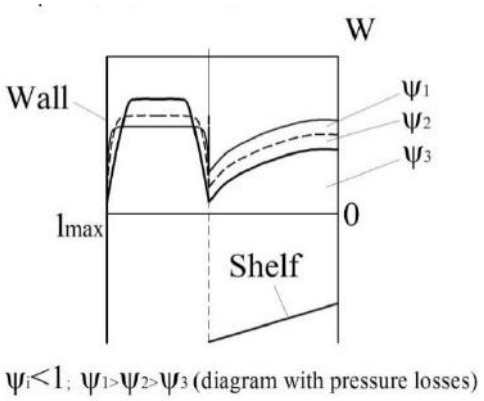

Figure 3 – Vertical velocity profiles over the shelf and in the outloading space, depending on the shelf perforation degree ψ (qualitative distribution)

As a result of the free cross-section narrowing of the vertical channel, the inclined perforated shelf installation in the workspace of the shelf device causes a local increase in the velocity and turbulence of the gas flow in the outloading space and a change in the profile of gas flow velocities under the surface of the shelf and above it. As can be seen from Figure 4 (curves 1 and 2), a decrease in the value of the L_{cl}/L_{dev} ratio from 0.5 to 0.15 significantly increases the uneven distribution of the gas flow over the section of the workspace in the device in comparison with the installation of the perforated grid completely overlying the section of the workspace in the device (an analogue of the fluidized bed device (Figure 4, curve 4)), or the free channel (a pneumatic tube device (Figure 4, curve 5)). In this case, the width of the zone where the gas flow comes through

the outloading space decreases, its absolute velocity and the profile of gas flow velocities in the workspace of the device is changed.

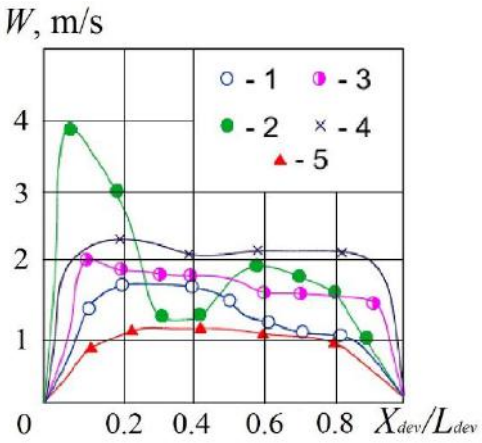

Figure 4 – The distribution of gas flow velocities along the section length of the device where the shelf is installed: 1—L_{cl}/L_{dev} = 0.5, ψ = 15%; 2—L_{cl}/L_{dev} = 0.15, ψ = 15%; 3—L_{cl}/L_{dev} = 0.15, ψ = 30%; 4—L_{cl}/L_{dev} = 0; 5—L_{cl}/L_{dev} = 1. Tilt angle of the shelf—γ = 25°. Gas flow velocity in the free cross-section—1.2 m/s

If L_{cl}/L_{dev} = 0.5 and the degree of the shelf perforation is 15% (Figure 4, curve 1) in the above-shelf space, the absolute values of the gas flow velocities are practically constant over the section of this space and reach a maximum only in the outloading space and above it. If L_{cl}/L_{dev} = 0.15 (Figure 4, curve 2) the velocity profile has two maximum values: in the zone above the outloading space and at the middle level of the inclined shelf. This fact is explained by the differential “dividing” effect of the inclined shelf on the profile of gas flow velocities in or another one quantity through the outloading space and the holes in the inclined shelf. In the first case, the inclined shelf does not cause such a significant unevenness in the profile of gas flow velocities in the workspace of the device beyond its input point. In the second case, due to an increase in the resistance to the gas flow, caused by a sharp narrowing of the free cross-section in the device, significant swirlings arise at the inclined shelf edge. It defines the presence of a zone with a reduced gas flow velocity in the space above the end of the shelf. An increase in the

perforation degree of the inclined shelf to 30% (Figure 4, curve 3) levels out the unevenness of the velocity profile over the cross-section of the workspace in the device since the gas flow is redistributed into the holes of the shelf due to a reduction of the hydraulic resistance of the shelf to its access.

A comparison of the experimental (Figure 4) and theoretical velocity profiles (Figure 3) shows a sufficient coincidence between the nature of the gas flow velocities change along the cross-section of the workspace in the device. The absolute value of the gas flow velocity in the outloading space with a decrease in the L_{cl}/L_{dev} ratio from 0.5 to 0.3 grows insignificantly for a shelf with a perforation degree from 0% to 30% (Figure 5).

Under the conditions of the further decrease in the L_{cl}/L_{dev} ratio up to 0.15, the gas flow velocity in the outloading space increases by 2.5–3 times in comparison with the average gas flow velocity in the free cross-section of the device. With a decrease in the perforation degree of the shelf cross-section, this growth is more significant since the hydraulic resistance to the gas flow through the holes of the shelf contact is increased and the gas flow is redistributed towards the outloading space. The gas flow velocity in the outloading space reaches its maximum value at $L_{cl}/L_{dev} = 0.15$ for shelves with a perforation degree from 0% to 30%. If $L_{cl}/L_{dev} < 0.15$, the gas flow velocity in the outloading space decreases since the hydraulic resistance to the gas flow through the outloading space is increased so much that most of the flow passes through the holes of the shelf. If the shelf contact has a perforation degree of 0% (solid shelf), there is no redistribution, and the gas flow velocity in the outloading space continuously increases with reduction of L_{cl}/L_{dev} ratio (Figure 5, curve 1).

A change in the constructive parameters of the shelf has a significant effect on the uneven profile of gas flow velocities. It is reasonable to represent its quantitative measure by the dimensionless coefficient of the gas flow uneven distribution n, which is the ratio of the gas flow passing through the outloading space Vo.s. to its quantity in the holes of the shelf V (Figure 6).

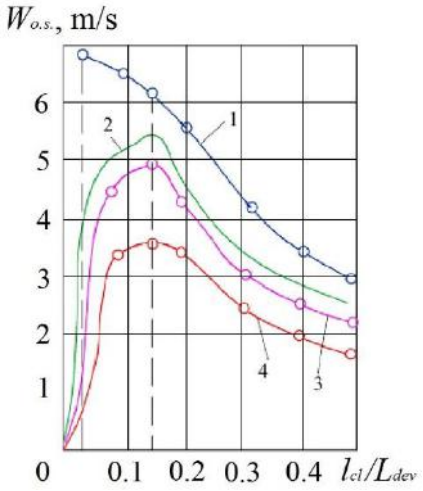

Figure 5 – The dependence of the gas flow velocity in the outloading space on the constructive parameters of the shelf. Shelf perforation degree ψ: 1–4—respectively, 0%, 5%, 15%, 30%. The tilt angle of the shelf—$\gamma = 25°$. Gas flow velocity in the free cross-section—1.65 m/s

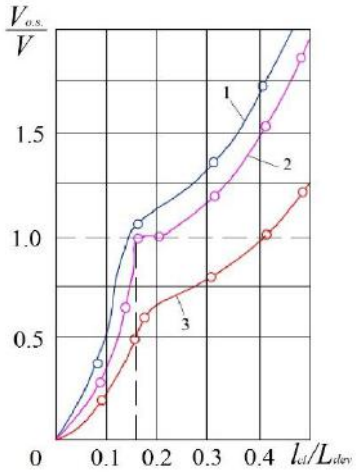

Figure 6 – The influence of the constructive parameters of the shelf on the uneven profile of gas flow velocities. Degree of the shelf perforation ψ: 1–3—respectively, 5%, 15%, 30%. The tilt angle of the shelf—$\gamma = 25°$. Gas flow velocity in the free cross-section—1.65 m/s.

If the coefficient of the gas flow uneven distribution is more than 1, the gas flow passes mainly through the outloading space, and if less than 1—through the holes of the inclined shelf. If the coefficient of the gas flow uneven distribution is 1, the flow is

distributed in equal amounts both through the outloading space and through the holes of the shelf.

The special nature of the gas flow distribution determines the conditions for the emergence of various hydrodynamic modes of interaction between solid particles in the material and the ascending gas flow. It enables widely to influence the heat treatment efficiency (for example, cooling and drying) of granular and grained materials in devices with inclined perforated shelves.

At low gas flow velocities, the material continuously fed into the device with a flow rate of 6 kg/(m^2·s) moves along the surface of the inclined shelf in the form of a rapidly "jumping" layer since the particles at the outlet of the supply pipe have sufficient inertia force. The porosity of such a layer reaches 0.8–0.85, and the concentration of material particles in it is 20–30 kg/m^3 (0.15–0.2 m^3/m^3). Particles of the material after moving along the inclined shelf surface with a velocity of 0.2–0.3 m/s are inhibited at the device wall in the outloading space and are accumulated on the wall surface (Figure 7a).

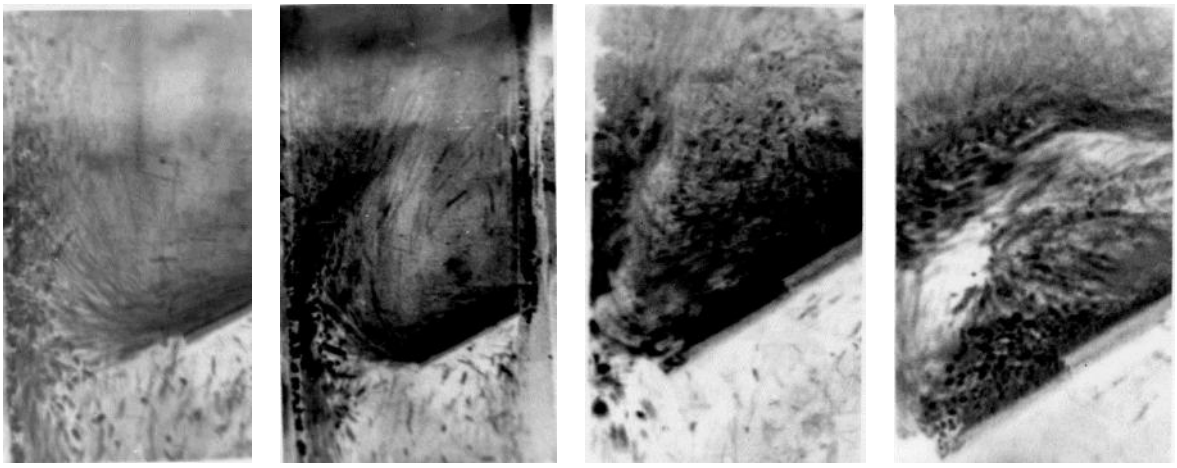

(**a**) (**b**) (**c**) (**d**)

Figure 7 – Photographic image of hydrodynamic modes: (**a**) "gravitationally falling layer" mode; (**b**) "transitional" mode; (**c**) "weighted layer" mode; (**d**) "piston" mode

The accumulated particles layer is blown by the ascending gas flow. Moreover, the layer mass due to the arrival of new portions of solid particles of material gradually

increases. At a certain point in time, it exceeds the aerodynamic force of the ascending air flow, after which some of the particles are fallen down the device through the outloading space. In this nature of the motion of the material particles, both on the inclined shelf surface and the outloading space, the aerodynamic forces of the ascending flow do not provide sufficient resistance to the motion of the solid particles. The main part of the material moves in the form of a thin layer through the outloading space mainly by gravitational forces. Therefore, this nature of the motion of the solid particles in the material was called the “gravitationally falling layer” mode.

By increasing the gas flow velocity, its impact on the material layer grows. It begins to weigh particles both on the shelf contact surface and near the surface of the device wall in the outloading space (Figure 7b). In this case, the porosity of the material layer moving along the surface of the inclined shelf decreases to 0.7–0.75, and the concentration of solid particles of the material increases accordingly to 80–150 kg/m^3 (0.25–0.3 m^3/m^3). This mode was called “transitional”.

If a certain velocity of the gas flow is reached, its effect on the material particles increases so much that their share in the upper part of the layer, breaks away from the wall surface. As a result of the breakaway of solid particles in the material, their concentration in this zone increases, the particles do not have time to get carried away by the gas flow to the upper part of the device and, losing their velocity, “fall” down onto the inclined shelf surface. Thus, a continuously circulating vortex layer of solid material particles is formed above the surface of the inclined shelf. Having reached a certain period, the formed circulating vortex layer of solid particles has a stationary state in its hydrodynamic structure and is characterized by a constant concentration of solid particles in the layer equal to 160–280 kg/m^3 (0.32–0.35 m^3/m^3). The porosity of such a layer is 0.65–0.68, which corresponds to the porosity of fluidized systems. At the same time, the material moves along the inclined shelf surface in the form of a dense layer blown by the gas flow, and in the form of a weighted intensely circulating layer in the zone above the outloading space (Figure 7c). The velocity of material particles motion on the inclined shelf surface in this mode is reduced to 0.05–0.15 m/s.

The above mechanism demonstrates the transition of the hydrodynamic mode of the "gravitationally falling layer" of the material into the "weighted layer" mode given the "transition" mode. The velocity at which such a transition occurs is called the critical velocity of the initial weighing. The empirical dependence of the type defines the critical velocity of the initial weighing:

$$\mathrm{Re}_{crit} = \mathrm{Re}_{o.s.}\left[1.19 \cdot lg(100 \cdot \psi) + 0.005\right]\left(\frac{L_{cl}}{L_{dev}}\right), \quad (15)$$

$$W_{crit} = \frac{\mathrm{Re}_{crit} \cdot \nu}{d_p}, \quad (16)$$

where L_{cl} is the distance between the end of the shelf and the wall of the device, m;

L_{dev} is the length of the cross-section side in the device, m;

ψ is the perforation degree of the shelf, %;

W_{crit}—critical velocity of the initial weighing, m/s;

d_p is the average diameter of particles being weighed, m;

ν is the kinematic coefficient of the gas flow viscosity, m^2/s;

$\mathrm{Re}_{o.s.}$—Reynolds criterion in conditions of particle hovering in a gas flow;

$\mathrm{Re}_{o.s.} = W_{o.s.}\, d_p/\nu$;

$W_{o.s.}$—medium velocity in conditions of particle hovering, m/s.

The "piston" mode for weighing material particles occurs in the workspace of the device with a further increase in the air flow velocity (Figure 7d). This mode does not work. It is characterized by the maximum gas flow velocity.

The influence of the gas flow velocity on the interphase heat transfer process intensity is represented by the dependence Nu = f (Re) (Figure 8).

One can see from the graph (Figure 8, line 1) that the interphase heat transfer intensity between the gas flow and particles for the "gravitationally falling layer" mode increases slightly with an increase in the gas flow velocity in the free cross-section of the device, at 40 < Re < 600. It is proved by the fact that the particles of material coming from the loading nozzle move along the surface of the shelf with a sufficiently high

velocity, the contact time of the particles with gas jets coming from the holes of the shelf is small. Owing to the insufficient contact time of the rapidly moving layer of material with the gas flow, the Nusselt criterion values obtained for the interphase heat transfer conditions on the inclined shelf surface under conditions of the "gravitationally falling layer" mode implementation in the workspace of the device come into the Nu < 5 area.

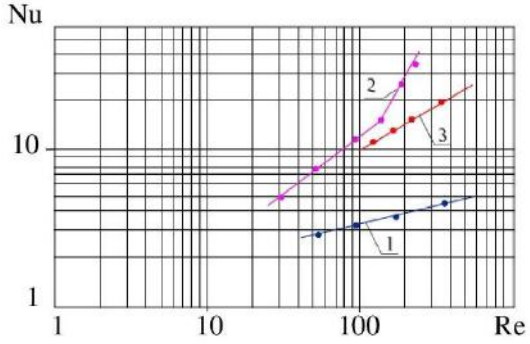

Figure 8 – The effect of gas flow velocity on the interphase heat transfer intensity: *1*—"gravitationally falling layer" mode; *2*—"weighted layer" mode; *3*—the fluidized bed on a horizontal grid

The empirical correlation for the "gravitationally falling layer" mode is the following [57]

$$Nu = 1{,}5 \cdot Re^{0.2} \text{ (if } 40 < Re < 600), \quad (17)$$

where the Nusselt criterion $Nu = \alpha \cdot d_p/\lambda_g$;

α—heat transfer coefficient from the surface of particles to the gas flow, W/(m^2·K);

λ_g—gas heat (thermal) conductivity coefficient, W/(m·K);

Reynolds criterion $Re = W \cdot d_p/v$;

W—gas flow velocity in the free cross-section, m/s.

The "weighted layer" mode initially (at Re = 30–170) is characterized by a gradual increase in heat transfer intensity, and then (at Re > 170) a significant increase in interphase heat transfer intensity is observed as a result of the material layer formation blown by the gas flow on the inclined shelf surface (Figure 8, line 2). This situation is

explained by the improvement of the conditions for “washing” particles with a gas flow, “opening” of their surface, and also due to additional turbulization of the boundary film as a result of an increase in the relative velocity of neighboring particles. In the weighted material layer in the area above the outloading space, the active heat transfer surface increases due to intensively circulating material particles throughout the entire weighted layer space. In the weighted layer mode, the most intensifying effect is exerted by a gas jet entering the weighted layer of material through the outloading space at a sufficiently high velocity. Due to the expansion of the gas flow at the exit from the space of the outloading gap, intense interaction is ensured over the entire area of the weighted layer in the filtration mode. When the material is unloaded, the lower part of the weighted layer partially overlaps the outloading space. It causes a slight increase in the gas flow velocity in this zone and its part is redistributed into the holes of the shelf. In this case, the uniform filtration mode of the material layer by the gas flow is replaced by the gas jet “breakthrough” through the material weighted layer over the outloading space. Therefore, such a variable mode defines the pulsating nature of the material particles interaction with the gas flow, not only in the layer of material weighted over the outloading space, but also in the layer moving along the inclined shelf surface. It increases the phase contact intensity, and, accordingly, the heat transfer coefficient in the weighted layer mode in comparison with the fluidized bed (Figure 8, line 3).

The experimental studies enabled to identify the “active” heat exchange zone of the shelf unit—the outloading space zone.

The empirical correlation for the “weighted layer” mode is the following [57]:

$$Nu = 0.38 \cdot Re^{0.73} \text{ (if } 30 < Re < 170), \quad (18)$$

$$Nu = 0.0045 \cdot Re^{1.73} \text{ (if } 170 < Re < 300). \quad (19)$$

Comparing the dependence, which is typical for the weighted layer on the inclined perforated shelf (Figure 8, line 2) with the dependence, which is peculiar for the fluidized

bed (Figure 8, line 3), we can see that the interphase heat transfer intensity in the former case is a bit higher.

It is difficult to identify the true residence time of solid particles in the weighted layers with different structures. That is why the authors propose a calculation method for estimating the average residence time of particles in a layer weighted above a shelf.

As can be seen from the trajectories of solid-phase motion in the photographs (Figure 7), the weighted layer can be divided into two zones: the solid particle motion zone on the surface of the shelf and the particle motion zone in the overshelf space.

For the first zone, the residence time of the particles is calculated by the formula:

$$\tau_1 = \frac{L_{sh}}{u_p \cdot (1-\beta)^m} = \frac{L_{dev} - \frac{L_{cl}}{L_{dev}}}{u_p \cdot (1-\beta)^m}, \quad (20)$$

where u_p is the velocity of solid particles motion on the shelf surface, m/s;

β—the volume concentration of the solid phase in the weighted layer, m^3/m^3;

m—the experimental coefficient;

m = 4.4–4.5—for the "weighted layer" mode;

m = 10–10.2—for the "gravitationally falling layer" mode.

The following empirical correlation is proposed to find the volume concentration of the solid phase in the weighted layer:

$$\beta = n \cdot G_{ex}^{0.95} \left(\frac{W}{W_{o.s.}} \right)^{0.6}, \quad (21)$$

where G_{ex} is the mass flow rate concentration, kg/kg;

$G_{ex} = G_p/G_{gas}$;

G_p—mass flow rate of the material, kg/s;

G_{gas}—mass flow rate of gas, kg/s;

W—velocity of the gas flow in free cross-section, m/s;

$W_{o.s.}$ is the velocity of medium diameter particles, m;

n is the experimental coefficient;

n = 0.25–0.35 for the “weighted layer” mode;

n = 0.1–0.15—for the “gravitationally falling layer” mode.

There is no weighted layer in the space above the shelf for the “gravitationally falling layer” mode, as can be seen from the photograph (Figure 7a). Therefore, the second zone is typical only for the “weighted layer” mode (photograph, Figure 7c). When particles pass along the shelf length, they meet with a gas jet, formed by the outloading gap. Particles with a velocity less than the velocity of the gas jet are carried up into space above the shelf. The velocity of the gas jet decreases in height. The particles with a velocity greater than the velocity of the gas are lowered down to the shelf surface. Only small particles are carried out by the gas flow from the device. Thus, in the second zone, the particles move up the trajectory to the upper boundary of the weighted layer and downward trajectory to the surface of the shelf. Then the residence time of the particles is calculated as the following:

$$\tau_2 = \frac{L_{tr}}{\vartheta_r} = \frac{2 \cdot k \cdot B_{dev}}{\vartheta_r}, \tag{22}$$

where L_{tr} is the length of the trajectory, m;

ϑ_r is the pulsation velocity of the solid particle, m/s;

k is the experimental coefficient;

$k = (1.5–3) \cdot B_{dev}$.

The pulsation velocity of a solid particle in a weighted layer is determined by the empirical dependence:

$$\vartheta_r = bW,\ 0 < W < 3.5 \text{ m/s}, \tag{23}$$

where b is the experimental coefficient, b = 0.06 (defined according to the regression with correlation coefficient of 0.844).

The calculations show that for the “weighted layer” mode with a gas flow velocity of 2.4 m/s in a free cross-section, the velocity of particles with average diameter of 2 mm is 10–12 m/s, the flow mass concentration of 3 kg/kg, the volume concentration of solid phase in the weighted layer 0.34 m^3/m^3 and the particle velocity on the surface of the shelf is 0.1 m/s, the residence time of the particle for the first zone is τ_1 = 5.73–5.97 s. For the second zone, at a pulsating velocity of particles in the layer of 0.14 m/s, the residence time is τ_2 = 2 s. The total estimated residence time of the particles in the weighted layer τ_Σ = 7.73–7.97 s. The experimental residence time of the particles in the layer (calculated as the ratio of the material amount in the weighted layer to its mass flow rate) is τ_{ex} = 7.72 s. For the gravitationally falling layer mode, the estimated time at a particle velocity of 0.25 m/s and a volume concentration of the solid phase in the layer above the shelf of 0.15 m^3/m^3 is τ_1 = 1.12–1.15 s, and experimental τ_{ex} = 1.16 s. The calculation results (Table 1) show that the residence time of the particles in the layer increases with the increase of the solid phase volume concentration in the layer and the number of shelves.

Table 1 – The residence time of solid particles in a shelf unit

Mode; Concentration β, m^3/m^3	**The Residence Time of Particles with Number of Shelves, s**				
	1	**2**	**3**	**4**	**5**
Weighted layer; 0.3	7.2	12.4	17.6	23.0	28.0
Weighted layer; 0.35	9.2	16.4	24.0	31.0	38.0
Gravitationally falling layer; 0.1	1.3	2.5	3.8	5.1	6.4
Gravitationally falling layer; 0.2	4.2	8.4	12.7	16.9	21.0

According to the comparative tests (Table 2) the shelf cooler-pneumoclassifier in terms of the cooling coefficient and the small fraction extraction degree exceeds pneumatic tubes devices, and units with fluidized and weighted layers, in which the specific cooling air flow rate to achieve the same cooling efficiency is 30–50% higher.

The temperature of the material in the device with one shelf (if L_{cl}/L_{dev} = 0.5) decreases from 90 to 65–70 °C. This insignificant cooling degree is explained by the short residence time of the material moving along the inclined shelf in the gravitationally falling layer mode. At the same time, as a result of the small concentration of material particles in the workspace of the device and the close contact of the particles with the air jet, a small fraction is intensively extracted from the product. The highest dusting degree is achieved with the shelf perforation degree of ψ = 5%. If the air flow velocity in the free cross-section of the device increases from 2.4 to 3.7 m/s, the extraction degree of the fraction of less than 1 mm in ablation is 30–60%, and the product fraction of 1–1.6 mm is not more than 1.5–2%.

Table 2 – Test results of a shelf cooler

Material	**Specific Productivity on the Material, kg/(m²·s)**	**Content of the Extracted Fractions Less Than 1 mm, %**			**Cooling Coefficient, K_{cool}**	**The Degree of Extraction, ε_m, %**	**Specific Air Flow Rate, m³/kg**	**Hydraulic Resistance, kPa**
		Initially	**In Ablation**	**In Undershooting**				
Ammophos	6	20	97.5	10	0.69	73	0.4	0.5–1.5
Superphosphate	6	40	100	26.2	0.6–0.65	50	0.4	0.5–1.5
	8	40	98	12.6	0.64–0.71	79	0.7	1.8–2.0

The cooling degree of the material on the shelf with a perforation degree of 15% and L_{cl}/L_{dev} = 0.5 increases significantly and reaches a maximum. If the specified optimal design parameters and air flow velocity in the cross-section of the device is 2.4 m/s, the “weighted layer” mode is implemented on the shelf, in which the particles are cooled more effectively, reaching a final temperature of 40–45 °C. As a result of the longitudinal mixing effect in this mode, the extraction efficiency of the small fraction is reduced to 20%.

The advantage of the shelf cooler-pneumoclassifier is the possibility to separate and to cool wide fractional composition materials without clogging grids and at low hydraulic

resistances not exceeding 1.5 kPa. Thanks to the pulsating outloading with the flow of the air share between the shelf perforation and the outloading gap and the intense phase contact in this space, a clear pneumatic classification is provided at high specific loads, reaching 15–20 kg/(m^2·s) significantly exceeding the specific loads of 0.1–1.5 kg/(m^2·s), at which fluidized bed coolers-separators work.

In the granular mineral fertilizer technology, cooling is used to stabilize the structure of the granules [58]. Thus, drum coolers are used, which reduce the temperature of NPK fertilizer granules from 60–80 to 30 °C [58]. The granules are also cooled using fluidized bed coolers [59]. A single-stage fluidized bed cooler for cooling doubled superphosphate provides cooling of granules from 85 to 40 °C with air at a temperature of 20 °C at a fluidization rate of 1.6 m/s, as well as cooling diammonitrofoska from 85 to 30 °C [60]. Therefore, according to the data in Table 2, the performance of the developed shelf cooler is fully confirmed.

Table 3 presents the testing results of the shelf dryers, which have significant advantages since the material is simultaneously separated and dried in such devices.

Table 3 – Testing results of the shelf dryer

Material	**Content of the Extracted Fractions Less than 0,1 mm, %**			**Extraction Degree, ε_m, %**	**The Humidity of the Material, %**			**Specific Productivity on the Evaporated Moisture, kg/(m^3·h)**
	Initially	**In Undershooting**	**In Ablation**		**Initial**	**Undershooting**	**Ablation**	
Fine-grained potassium chloride	7.5–10	1.2–5.5	60–80	80–90	6.1	0.1	0.06	420–460
Coarse-grained potassium chloride	4.5–10	2–5	58–65	70–80	7.0	0.14	0.1	520–1170

Thus, the content required in the dust-free product of a fraction of fewer than 100 μm in size equal to 1–2% is achieved for fine-grained potassium velocities at a flow

velocity of 1.44 m/s, and coarse-grained 1.34 m/s. If the flow velocity is more than 1.5 m/s in the coarse-grained potassium chloride, a fine-dispersed fraction is practically absent. The ablation of the fine-dispersed fraction of the material into cyclones does not exceed 6.5–10.8%, and the content of a fraction of more than 100 μm in it is 3–5%. The indicated results were achieved with specific loads on the section of the device in the material equal to 10 kg/(m^2·s), the hydraulic resistance of 700–1500 Pa, and specific gas flow velocity of 0.12–0.14 m^3/kg. For fluidized bed dryers, the ablation of the fine-dispersed fraction up to 7% is ensured at a gas velocity of 1.8–2.3 m/s. In this case, the specific gas flow rate is 0.41–0.52 m^3/kg, the hydraulic resistance is 1500–2500 Pa.

In the potassium chloride production technology, fluidized bed dryers provide drying of the product from an initial moisture content of 3–9% to a final moisture content of 0.1% [61]. Therefore, according to the data in Table 3, the developed shelf dryer's performance is fully confirmed.

To define the optimal number of experiments and the highest accuracy degree and reliability of the obtained results, as well as for the processing of these results, methods of mathematical statistics were used [62].

Two types of measurement errors—random and systematic—may occur during the experiment conducting [62].

A random error reduces the accuracy of experiment results. An analysis of this type of error is possible by using the root-mean-square deviation σ, calculated by the following equation:

$$\sigma = \sqrt{\frac{\sum_{i=1}^{n}\left(\bar{x} - x_i\right)^2}{n-1}}, \quad (24)$$

where $\bar{x}$ is the arithmetic mean value;

x is the single parameter value;

n is the number of measurements.

The maximum possible error of a single measurement, Δ, was determined by the three sigma rule:

$$\Delta = 3 \cdot \sigma . \tag{25}$$

The bilateral confidence interval of the arithmetic mean value ε was determined by the following function [62], provided that this parameter is located in the confidence interval with the probability not less than 95%:

$$\varepsilon = t \cdot \frac{\sigma}{\sqrt{n}}, \tag{26}$$

where *t* is the Student's criterion [63].

The root-mean-square error of indirect measurements is calculated as:

$$\sigma_y = \sqrt{\sum_{i=1}^{n} \left(\frac{\partial y}{\partial x} \Delta x_i \right)^2}, \tag{27}$$

where $y = f(x_1, x_2, \ldots x_n)$.

The accuracy of the obtained regression equations is determined by the least-squares method [64].

The systematic measurement error had an identical effect on all parameters that were controlled during the experiment. All measurement devices were calibrated by calibration instruments by comparing their accuracy with that declared in the technical documentation in order to exclude the above error. Connection between measurement devices and controllers was provided with a maximum error of processing signals within 1.5%.

Creation of graphical dependences was carried out by differential methods of mathematical analysis and integral calculus. Reliability of the obtained experimental results is due to application of time-tested methods in practice.

1. Due to the creation of an active hydrodynamic mode to weigh solid particles in a layer, a multistage fluidized bed device with inclined perforated shelves provides efficiency to carry out heat-mass transfer processes.

2. Changes in the constructive parameters of the inclined shelf (the width of the outloading space and the shelf perforation degree) identify the different nature of the gas flow distribution between the holes of the shelf and the outloading space.

3. Various hydrodynamic modes during operation of the device were revealed: the “gravitationally falling layer” mode and the “weighted layer” mode. The first mode is effective in carrying out pneumatic classification processes, and the second—in cooling and drying of granular materials.

4. The study of interphase heat transfer showed a higher intensity of heat transfer in the weighted layer on an inclined perforated shelf compared to a traditional fluidized bed on a horizontal gas distribution grid.

5. The theoretical model enables to present the gas flow velocity profiles depending on the length and perforation degree of the shelf contact, as well as to estimate the residence time of material particles in the workspace of the device.

6. Further research will point to develop the mathematical model of the weighted layer hydrodynamics on an inclined perforated shelf. The corresponding scientific and methodological approaches based on using artificial neural networks for parameter identification of the proposed mathematical model will be developed.

2 EXPERIMENTAL-INDUSTRIAL IMPLEMENTATION OF THE TECHNOLOGY FOR PRODUCING NANOPOROUS LAYERS ON AMMONIUM NITRATE: THE FINAL DRYING STAGE IN MULTISTAGE DEVICES

The ammonium nitrate, used as a component of industrial explosives, must have a developed network of nanopores on the surface for the liquid fuel (for example, diesel distillate) successfully to access the near-surface layers and the core of the granule. It is called a porous ammonium nitrate which is an integral part of the ANFO industrial explosive [65, 66].

The main methods of obtaining porous ammonium nitrate (PAN) are presented in various works, for example [67-73]. The ordinary ammonium nitrate granule humidification with its subsequent heat treatment, implemented in a vortex granulator [74-76], should be distinguished among other methods. This method has the following advantages:

1. Absence of pore-forming and modification additives in the formation of the porous structure in the granule.

2. Absence of phase changes in the granule and the formation of new compounds.

3. High strength of granules due to the minimum number of heat treatment cycles.

4. A developed network of twisting nanopores on the granules' surface due to a properly selected humidifier (for example, the water solution of ammonium nitrate).

5. Sufficient oxygen in the granule to detonate ANFO.

However, given the hydroscopic property of PAN granules (as well as any ammonium nitrate in general), it is essential to ensure a low value of residual moisture in the granules. This indicator is not normative (in contrast to the strength of the granule and retentivity and absorptivity concerning the diesel fuel distillate), but it influences the ANFO quality.

Excessive humidity of PAN granules leads to the following structural defects and a decrease in quality indicators:

1. Insufficient absorptivity of the granule.
2. Caking during storage and transportation.
3. Loss of strength.
4. Violation of the structure of nanopores.

Fig. 1 demonstrates the disturbance of the nanopores structure during storage of undried PAN. Several parts of the surface are "smoothed"; the pores disappear. This process leads to the fact that there are obstacles to the penetration of diesel distillate into the core of the granule. The relative porous surface area decreases, and the diesel fuel distillate flows from the granule already at the saturation stage (not to mention the storage and transportation of ANFO).

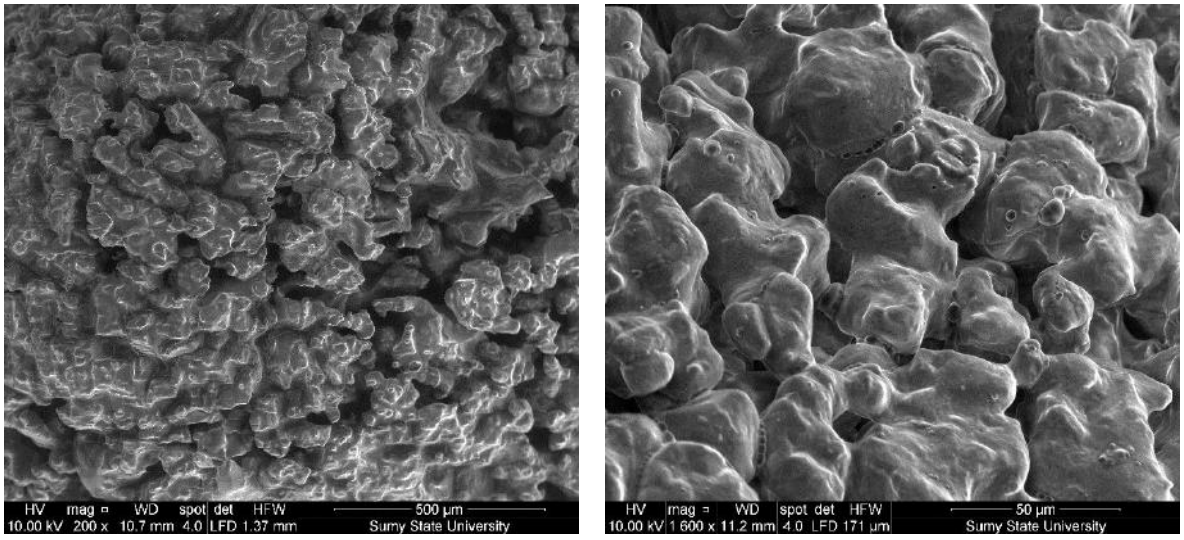

Figure 9 – Disturbance of the PAN granule nanoporous structure with its excess humidity

Therefore, the study [72] proposes an improved scheme for PAN production, which includes an additional final drying stage.

Drying methods are diverse in the way of realization, organization of flow, instrumentation, the use of extra stages, etc [77-83]. The data analysis from the above sources and data [84-88] enables an improved design of the drying unit - a multistage gravitational shelf dryer [89].

Thus, the finally improved scheme for PAN production with the final drying stage is in Fig. 9. This scheme was first proposed in [90], where it was the first time the granule samples after final drying were studied.

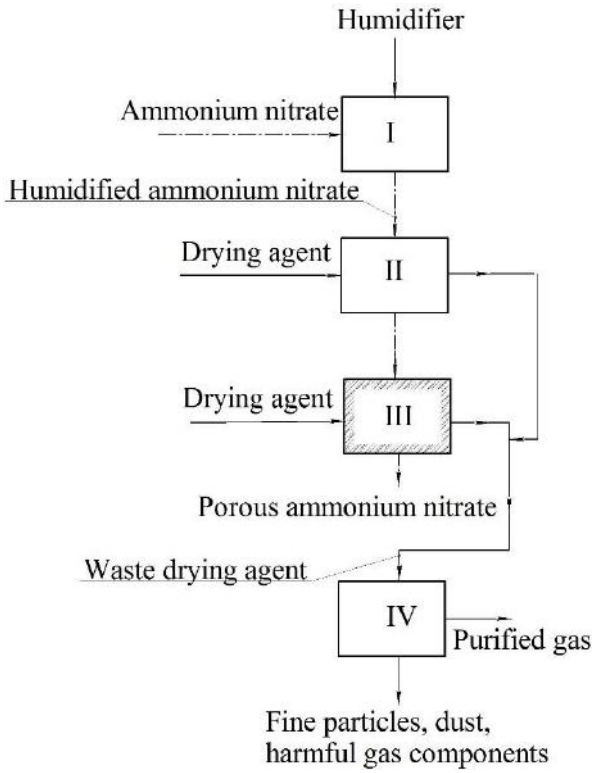

Figure 9 – Scheme of PAN production [90]: 1 – humidification of ordinary ammonium nitrate granules; 2 - granulation-drying; 3 - final drying; 4 - purification of exhaust gases

It is necessary to solve two problems for the successful implementation of the improved method within the framework of this work:

1. To model the heat treatment and dehydration of PAN.

2. To confirm the efficiency of the final drying stage to form a developed nanoporous structure of the PAN granule.

The scheme of the experimental stand for the final drying stage of the PAN is shown in Fig. 10.

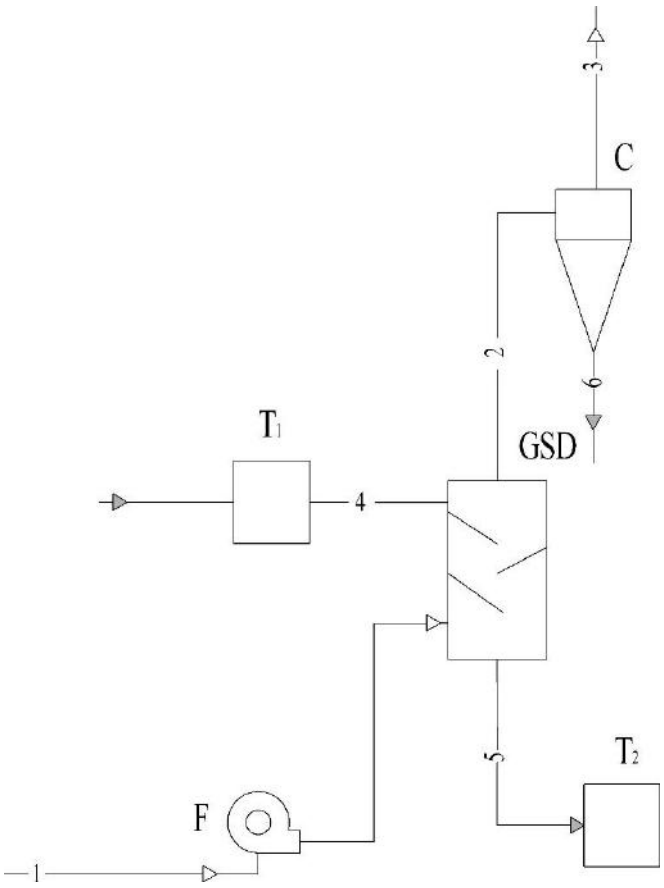

Figure 10 – Schematic diagram of the experimental stand for the study of shelf devices: F – fan; GSD – gravitational shelf unit; C – cyclone; T1, T2 – containers (tanks); 1 – drying agent; 2 – waste drying agent; 3 – purified gas; 4 – PAN; 5 – PAN after final drying; 6 – fine particles

The surface morphology of the granules is studied by scanning electron microscopy using a SEO-SEM Inspect S50-B instrument.

The Converter Image tool, with its interface in Fig. 11, is investigated to analyze the scanning electron microscopy results (pore size, shape, relative porous surface area, etc.). This tool enables to modify images to determine the surface relief and detailed study of the pore structure.

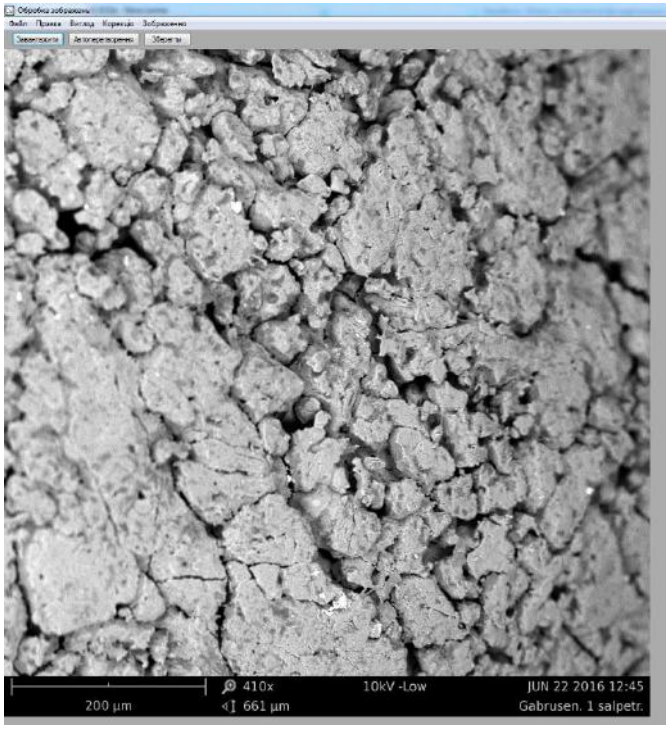

Figure 11 – The interface of the author's program for studying the nanoporous surface morphology of granules with the initial results of microscopy
(the interface language is Ukrainian)

When considering the drying process kinetics of a single spherical particle, interphase heat exchange process between its surface and the drying agent flow is observed at the first level as well as heat transfer inside.

When the nature of thermal conductivity inside the particle affects the moisture removal kinetics, the calculation is based on the equations of internal heat and mass transfer [91]:

$$\left.\begin{aligned} \frac{\partial t_m}{\partial \tau} &= a_{td}\left[\frac{\partial^2 t_m}{\partial r^2}+\frac{2}{r}\frac{\partial t_m}{\partial r}\right]+\frac{\varepsilon^* r_{ph}}{c_p}\frac{\partial U_m}{\partial \tau} \\ \frac{\partial U_m}{\partial \tau} &= k\left[\frac{\partial^2 U_m}{\partial r^2}+\frac{2}{r}\frac{\partial U_m}{\partial r}\right]+k\sigma^*\left(\frac{\partial^2 t_m}{\partial r^2}+\frac{2}{r}\frac{\partial t_m}{\partial r}\right) \end{aligned}\right\}, \quad (28)$$

where t_m – temperature of the material;

U_m – relative humidity of the material;

ε^* – phase transformation criterion;

σ^* – thermogradient moisture transfer coefficient;

a_{td} – thermal diffusivity coefficient;

r_{ph} – specific heat of phase transition;

r – the current radius of PAN granules;

c_p – heat capacity of the PAN granule;

k – potential conductivity coefficient.

According to the mass transfer equation, the drying process calculation has some peculiarities since an interconnected heat and mass transfer process occurs in the drying objects: moisture removal and simultaneous heating of the wet material. There is a relationship between these processes since the mass transfer coefficients depend on the temperature, and heat - on the moisture in the material [92].

Given that at each stage, the material is dried in a limited range of humidity and is thermolabile, it is also advisable to assume the analogy of gradient mechanisms of heat and mass transfer. Then the system of equations (28) is as follows:

$$\left.\begin{aligned} \frac{\partial t_m}{\partial \tau} &= a_{td}\left[\frac{\partial^2 t_m}{\partial r^2} + \frac{2}{r}\frac{\partial t_m}{\partial r}\right] \\ \frac{\partial U_m}{\partial \tau} &= k\left[\frac{\partial^2 U_m}{\partial r^2} + \frac{2}{r}\frac{\partial U_m}{\partial r}\right] \end{aligned}\right\}, \tag{29}$$

Using one of the system equations (29) as one of the author's describing methods proposed [91] to calculate the drying kinetics, makes it possible to replace the second equation with an empirical approximation. Thus, the temperature-humidity feature of the material closes the system of heat and mass transfer equations. For drying process calculation in the concentration zones, in this case, it is necessary to know the thermophysical properties of the dispersed material. Moreover, one can use a similar temperature-humidity approximation to define the mass transfer coefficient and mass transfer properties.

Currently, there are many theoretical solutions of heat and mass transfer differential equations for dispersed systems that can be dried [93, 94]. All of them describe the

heating process of particles under given third kind initial and boundary conditions in equations (29).

We consider one of the most common exponential models [95] through changes in temperature and humidity of the particle depending on its current radius and drying time:

$$\frac{t_{(r,\tau)} - t_{dr.in}}{t_{dr.in} - t_{m.in}} = 1 - \sum_{n=1}^{\infty} A_n \frac{\sin \mu_n \frac{r}{R}}{\mu_n \frac{r}{R}} \exp\left(-\mu_n^2 Fo_t\right), \tag{30}$$

$$\frac{U_{m.in} - U_{(r,\tau)}}{U_{m.in} - U_{dr.in}} = 1 - \sum_{n=1}^{\infty} A_n \frac{\sin \mu_n \frac{r}{R}}{\mu_n \frac{r}{R}} \exp\left(-\mu_n^2 Fo_u\right), \tag{31}$$

where $t_{(r,\tau)}$ – the temperature of the particle in its current radius at a given time;

$t_{m.in}$ – the initial temperature of the PAN granules, which are getting dried;

$t_{dr.in}$ – the initial temperature of the drying agent, °C;

$U_{m.in}$ – the initial moisture content of the PAN granules, which are getting dried;

$U_{(r,\tau)}$ – the humidity of the particle in its current radius at a given time;

$U_{dr.in}$ – the initial humidity of the drying agent;

R – the peculiar size of the dispersed material;

Fo_t – Fourier test for heat transfer during drying process;

Fo_u – Fourier test for mass transfer during drying process;

A_n, μ_n – constant coefficients and roots of the characteristic equation, the values of which are in the relevant tables [96].

The root of characteristic equations (30)-(31) μ_n is a Biot criterion function

$$\mu_n = f\left(Bi\right), \tag{32}$$

calculated by the following formula:

$$Bi = \frac{\alpha \cdot R}{\lambda}, \tag{33}$$

where α – heat transfer coefficient;

λ – thermal diffusivity coefficient.

When considering this functional dependence, the features of the heat transfer process, determined by the limit values of the Biot criterion, are considered:

$$0 < Bi < \infty, \tag{34}$$

If $Bi \to 0$ the small dispersed material will have the maximum thermal diffusivity, if $Bi = \infty$ the material of the maximum size will have the maximum heat transfer coefficient.

Based on the limit values of the Biot criterion for the drying process, it is necessary to use it within the specified limits to find the root of the characteristic equation (30) μ_n.

The heat transfer coefficient α for determining the Biot criterion is obtained from experimental data obtained by the authors [97]. Depending on the Biot criterion, the root of the equations (30)-(31) μ_n is determined on the graph [91].

One should note that solutions (30) - (31) in the form of series are found quickly. Starting with some value of the Fourier criterion, calculation accuracy of 1-2%, acceptable in engineering practice, can be achieved thanks to the first two or three members in the series. In this case, the contribution of the first member of the series is not less than 96%, i.e., the error will not exceed 3-4%. Thus, given the conditions

$$\left.\begin{array}{l} r = R, \\ Fo \geq 0,7 \end{array}\right\}, \tag{35}$$

from the equation (30), the heating kinetics of the particle is determined by the exponential function:

$$\frac{t_{surf}-t_{m.in}}{t_{dr.in}-t_{m.in}}=1-A_n\cdot\frac{\sin\mu_n}{\mu_n}\cdot\exp(-\mu_n^2\cdot Fo_t), \quad (36)$$

where t_{surf} – the temperature of the PAN granule surface;

Given the value of the Fourier test, the equation (36) is as follows:

$$\frac{t_{surf}-t_{m.in}}{t_{dr.in}-t_{m.in}}=1-A_n\cdot\frac{\sin\mu_n}{\mu_n}\cdot\exp(-\mu_n^2\cdot\frac{a_{td}\cdot\tau_h}{R^2}), \quad (37)$$

where τ_h – heating time.

The exponential nature of the surface temperature change in the dispersed particle according to equation (37) is shown in the graphs (Fig. 12).

Analysis in Fig. 12 shows that the material is heated with different intensities at a constant radius of the particle, depending on its thermophysical properties. The particles with similar thermophysical properties are heated more intensely when their radius decreases.

Given the active mixing of particles in the layer, the drying process kinetics is described by the balance equations of heat and moisture transfer in the fluidized bed of solid particles:

$$\begin{cases} G\cdot c_p\cdot\rho_p\dfrac{dt_m}{d\tau}=\alpha\cdot F_{gr}(t_{dr}-t_m) \\ \rho_p\dfrac{dU_m}{d\tau}=\beta\cdot F_{gr}(U_m-U_{dr}) \end{cases}, \quad (38)$$

where G – flow concentration (as the ratio between mass flow rates of solid and gas phases);

ρ_p – density

U_m – current humidity of the material;

t_m – current temperature of the material;

t_{dr} – the current temperature of the drying agent;

β – mass transfer coefficient;

F_{gr} – the specific surface area of the PAN granules in the device $F_{gr} = \frac{6(1-\varepsilon)}{d}$;

τ_{dr} – drying time of the material.

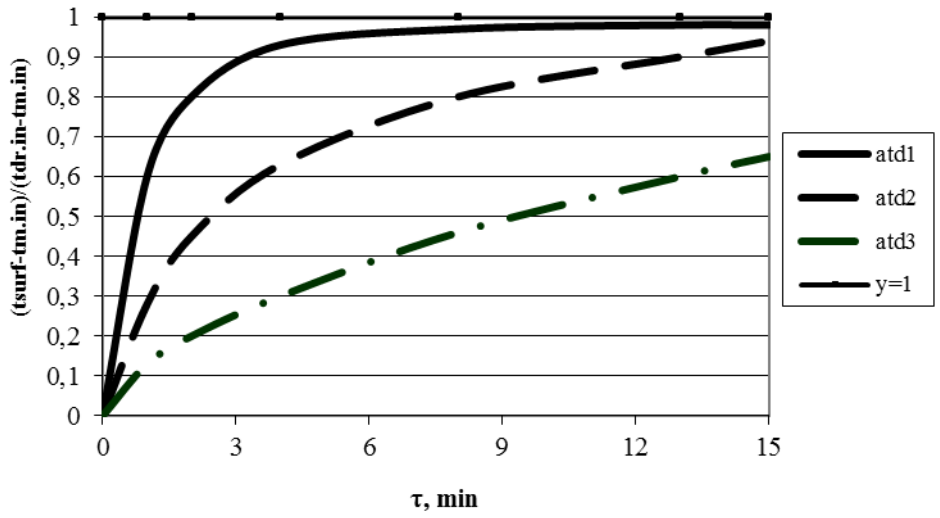

a

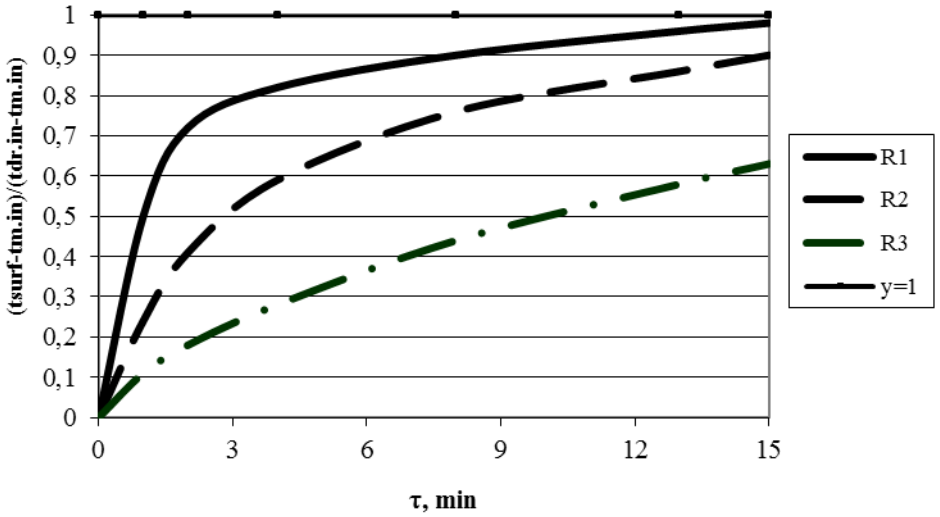

b

Figure 12 – Qualitative nature of intensity curves of the material heating: a – if R = const depending on their thermophysical properties $(a_{td1} > a_{td2} > a_{td3})$; b – if $a_{td} = const$ depending on their thermophysical properties $(R_1 < R_2 < R_3)$

After integration of the equation (38), we obtain:

$$\begin{cases} \dfrac{t_{dr.in}-t_m}{t_{dr.in}-t_{m.in}} = \exp\left(-\dfrac{\alpha \cdot F_{gr}}{G_в \cdot c_p \cdot \rho_p} \cdot \tau_h\right) \\ \dfrac{U_m - U_{dr.in}}{U_{m.in} - U_{dr.in}} = \exp\left(-\dfrac{\beta \cdot F_{gr}}{\rho_p} \cdot \tau_{dr}\right) \end{cases}, \tag{39}$$

A linearization defines the kinetic features of these exponential curves. Thus, equations (39) show that the heating rate of a material with a peculiar particle size d is a parameter K_t:

$$K_t = \frac{\text{a}}{G Ч_p Ч_p} ч \frac{6(1-\varepsilon)}{d}., \tag{40}$$

The first equation of the system (39), considering the replacement of the corresponding parameters in the left part of this equation, will be as follows

$$\frac{t_{dr.in}-t_m}{t_{dr.in}-t_{m.in}} = \exp(-K_t \tau_h), \tag{41}$$

or after logarithmation

$$K_t \tau_h = -\ln \frac{t_m - t_{m.in}}{t_{dr.in} - t_{m.in}}, \tag{42}$$

Thus, after linearization, the heating kinetics model becomes convenient for processing the statistical data and determination of kinetic parameters (Fig. 13 a). Table 4 demonstrates the data for the construction of the following graphical relationship.

This graph shows that the kinetic parameter K_t is the tangent of the tilt angle of the line, approximating the experimental points in the coordinates of time and dimensionless temperature.

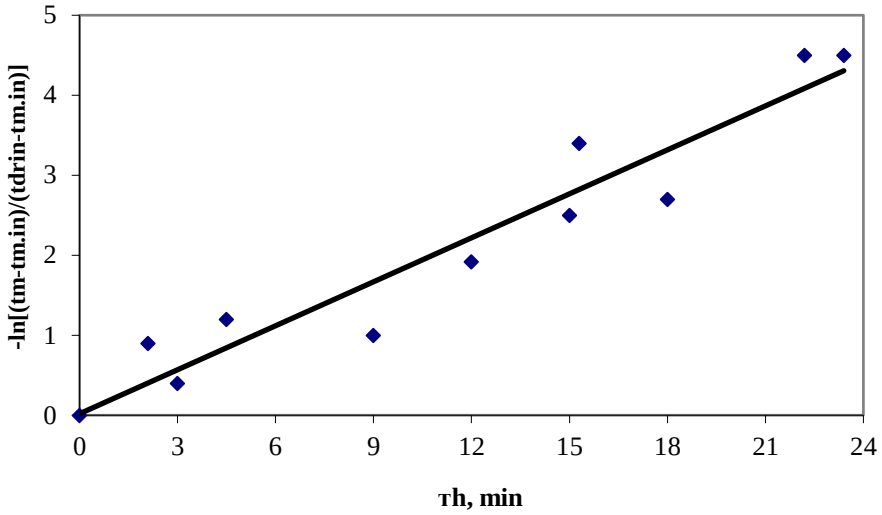

a

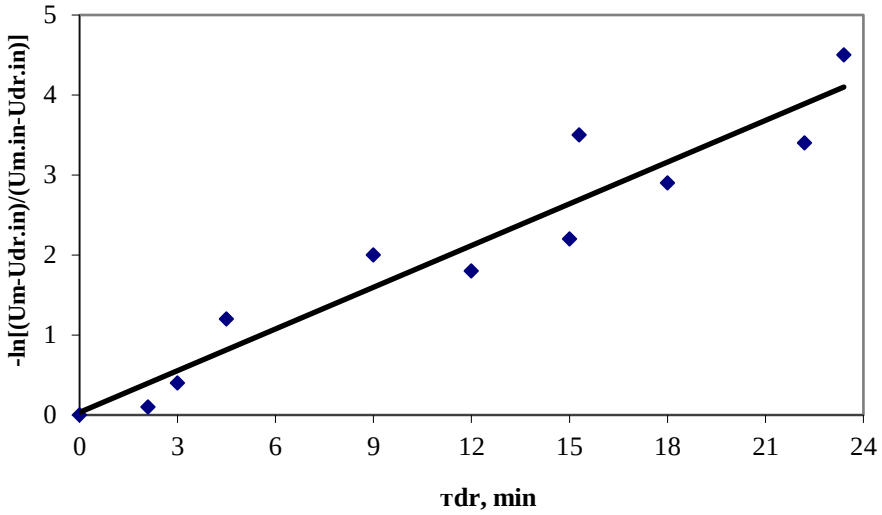

b

Figure 13 – Graph of the kinetic parameter: a – for heating of the material (K_t); b – for drying of the material (K_u)

It is reasonable to investigate the change in material humidity according to a similar solution (41) with the appropriate replacement of temperatures by humidity, to find the drying time of the dispersed particle.

Table 4 – Data of the kinetic parameter for the material heating

Value $-\ln\frac{t_m - t_{m.in}}{t_{dr.in} - t_{m.in}}$	Heating time τ_h, min
0	0
1,2	4,5
1,0	9,0
1,92	12
3,4	15,3
2,7	18
4,5	23,4
0,9	2,1
2,5	15
0,4	3
4,5	22,2

The linearized graph of drying kinetics in time and humidity coordinates is represented in Fig. 13 b. Table 5 demonstrates data for the construction of the following graphical relationship.

Table 6 – Data of the kinetic parameter K_u for the material drying

Value $-\ln\frac{U_m - U_{dr.in}}{U_{m.in} - U_{dr.in}}$	Drying time τ_{dr}, min
0	0
1,2	4,5
2,0	9,0
1,8	12,0
3,5	15,3
2,9	18,0
4,5	23,4
0,1	2,1
2,2	15,0
0,4	3,0
3,4	22,2

According to the analogy of heat and mass transfer processes, the linear approximation equation of the humidity change is like (15)

$$K_u \tau_{dr} = -\ln \frac{U_m - U_{dr.in}}{U_{m.in} - U_{dr.in}}, \quad (43)$$

where $K_u = \frac{\beta \Psi F_{gr}}{\rho_p}$ – kinetic parameter of moisture transfer.

Based on the initial humidity of the material, the drying agent and the required technological humidity of the material, the drying time is calculated

$$\tau_{dr} = -\frac{1}{K_u} \ln \frac{U_m - U_{dr.in}}{U_{m.in} - U_{dr.in}}, \quad (44)$$

There are many studies regarding the surface morphology of the PAN granule to confirm a developed network of nanopores on the surface of the granules after the final drying stage. The PAN granule is taken as a sample for comparison after humidification and heat treatment in the vortex granulator (Fig. 14). The sample of PAN granules after the vortex granulator has a network of shallow nanopores. Some of the pores are cavities on the surface and cannot transport diesel fuel distillate deep into the granule (Fig. 14a). Being humidified, the liquid will flow out of these cavities. The retentivity of the granule (if there are many such pores) will be low and will not provide a regulatory indicator.

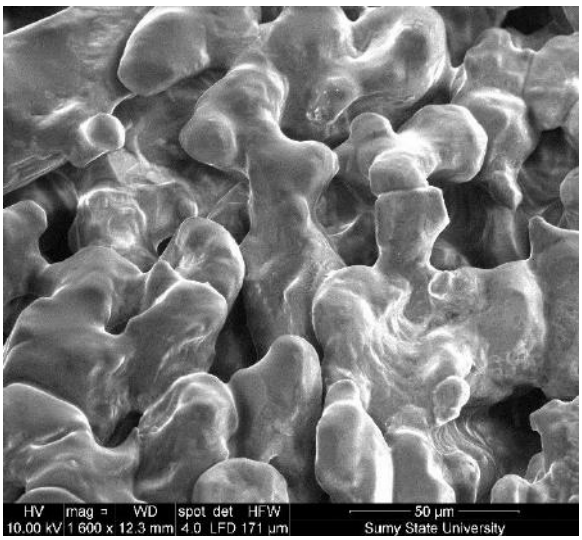

a

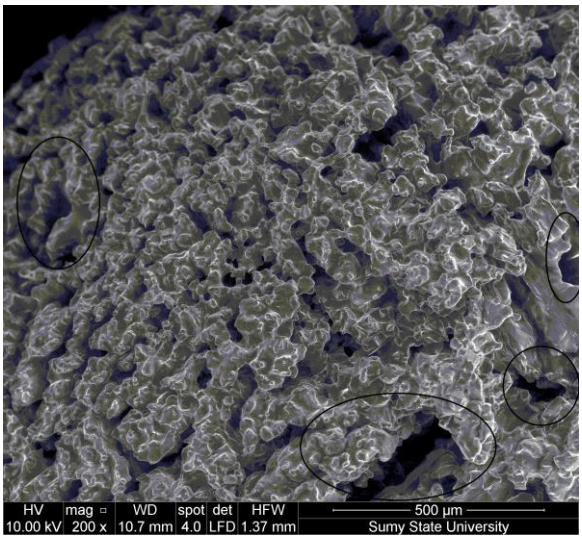

b

Figure 14 – PAN granule after humidification and heat treatment in a vortex granulator (a) and "mechanical" pores on its surface (b)

Although the number of such cavities is about 10% of the total surface area, this index should be reduced to 3-4%. In this case, these cavities will not significantly affect the retentivity of the granule. One should also note that there are "mechanical" pores - faults and cracks on the PAN granules after the vortex granulator, caused by the internal temperature stresses and during vaporization in the heat treatment process (Fig. 14b). The "mechanical" pores will not disappear after the final drying. However, their relative number may decrease due to the formation of new nanopores.

Another disadvantage of this sample is the number of twisting micropores (in the nanometer range), making 30-40% of the total number of nanopores. There are also many mesopores (up to 25%). The rest of the pores are macropores. Besides, the pores are predominantly rectilinear on the surface of the PAN granules. It facilitates the penetration of diesel fuel distillate into the granule. However, it reduces the leakage of this liquid influenced by the external forces (starting from gravity). This pore size distribution and pore shape do not significantly affect the ANFO quality preparing this industrial explosive directly on site. However, the long-term storage or transportation to the blasting places through such pores lead to the leakage of the diesel fuel distillate. Besides, these pores can cause the caking of PAN granules since the moisture easily penetrates the near-surface layers and destroys the surface.

Thus, after the final drying stage, it is necessary to increase the number of micropores, and eliminate the cavities substituting them with a network of deep twisting pores.

We consider the nanoporous surface structure of the PAN granules after the final drying stage in a multistage gravitational shelf unit (Fig. 15). There are twisted and deep nanopores of different sizes on the surface. One should note the increase in pore depth compared to the PAN sample after the vortex granulator. The granule surface structure is changed in direction of reducing the number of cavities and replacing them with deep pores, increasing the tortuosity of the nanopores, their number and relative area of the porous surface.

The data below show the study regarding the properties of the samples.

1. The method of obtaining the sample: humidification and heat treatment in a vortex granulator.

Strength of the granule, kg / granule - 0.43.

Absorptivity, % –12.2.

Retentivity, % - 8.5.

The relative number of "mechanical pores", % - 14.

Number of nanopores, % (micropores / mesopores / macropores) - 40/25/35.

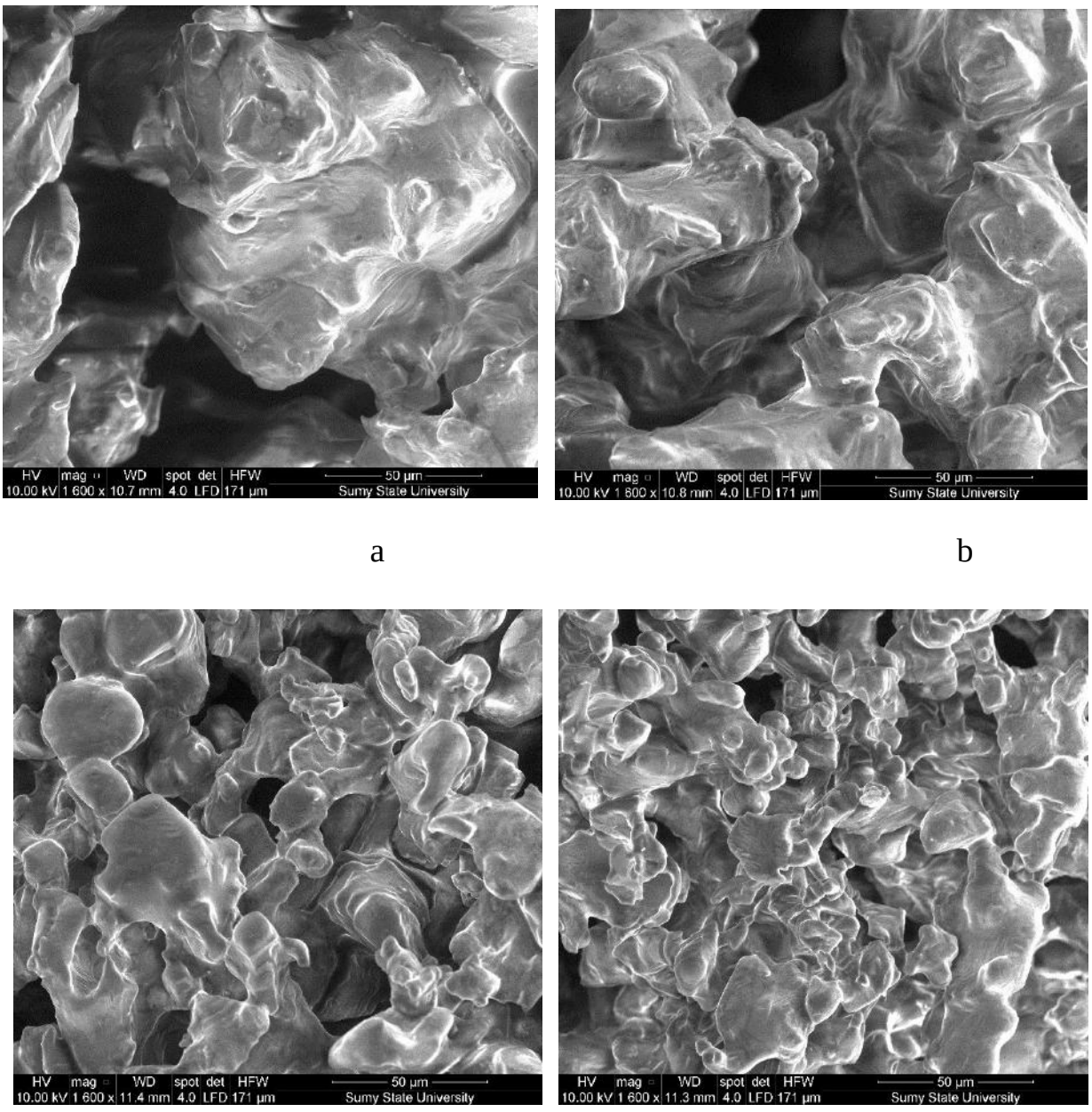

Figure 15 – PAN granule after the final drying stage: a - "mechanical" pores; b - macropores; c - mesopores; d - micropores

Relative number of cavities, % - 10.

The relative area of the porous surface, % - 70.

2. The method of obtaining the sample: humidification and heat treatment in a vortex granulator + final drying

Strength of the granule, kg / granule - 0.43.

Absorptivity, % –13.

Retentivity, % - 9.1.

The relative number of "mechanical pores", % - 10.

Number of nanopores, % (micropores / mesopores / macropores) - 60/30/10.

Relative number of cavities, % - 6.

The relative area of the porous surface, % - 77.

Analysis of these data enables us to draw the following conclusions:

1. After the final drying, the strength of the granules does not decrease since a new cycle of heat treatment does not occur, and the granule continues to dry at the same temperature.

2. The absorptivity value increases since instead of cavities on the granule, there are deep nanopores, which allow the diesel fuel distillate to penetrate deep into the granule.

3. The retentivity value increases since the number of twisting deep micropores increases. These micropores allow the diesel distillate to penetrate deep into the granule and stay securely there.

4. The relative number of mechanical pores decreases since the total number of micropores / mesopores / macropores increases.

5. Some cavities on the surface of the granules are replaced by nanopores of different sizes.

6. The ratio of micropores / mesopores / macropores changes increasing micropores.

7. The relative surface area of the porous surface increases slightly but the porous surface structure undergoes significant changes.

3 DRYING MACHINES WITH COMBINED HYDRODYNAMIC REGIMES

Scheme of multistage shelf dryer is shown in fig. 16.

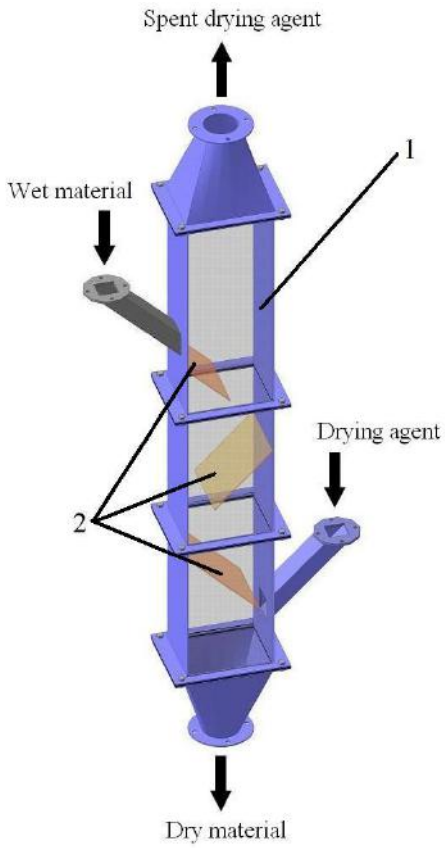

Figure 16 – Multistage shelf dryer: 1 – case; 2 – shelf

Its working principle is as follows [98].

To the bottom side-bar of case 1 drying agent is supplied. The drying agent is distributed evenly over the cross-section of the case and then rises up. As the drying agent moves up on the case, it consistently passes through the cross-sections of the lower side-bar, middle side-bar and top side-bar, tapered side-bar is withdrawn from the device.

Length of shelf provides a residence time of dispersed material, which promotes complete heating of the material, separating of small dispersed particles and unbound moisture remove from the top surface layer of dispersed material in the period of constant speed of drying.

Dispersed material during drying flow of drying agent gradually moves the top shelf is withdrawn from it on the middle shelf (further intensive removal of unbound water from the surface of the layer of dispersed material during the period of constant speed of drying) and then on the bottom shelf (remove bound water from the depth of the material in the period of falling speed of drying).

After passing all shelves dispersed material was withdrawn from the bottom part of the dryer.

For a theoretical description of the drying process in a shelf dryer, a mathematical model [99] is proposed, consisting of three consecutive levels. The time for drying the dispersed material to the required final moisture content is determined at the first level. The second level of the model is devoted to describing the hydrodynamics of the process; the residence time of particles in the apparatus is determined, which is compared with the drying time from the first level. At the third level, a recurrent calculation of removing moisture from the material in the volume of the entire apparatus is carried out, the efficiency of each stage of the apparatus and the optimal design parameters of the dryer are determined.

By varying the design parameters of the shelf (angle of inclination, the gap between the end of the shelf and the wall of the apparatus, the free section area and the diameter of the perforation holes of the shelf), it becomes possible to determine their optimal values to achieve maximum drying efficiency at each stage of the apparatus.

Due to changes in the design parameters of the shelf contacts of the dryer, the necessary hydrodynamic conditions for the movement of material on each shelf of the cascade are provided. Note that when designing a gravity shelf dryer, it is necessary to ensure uniform contact of the drying agent with the dispersed material on each shelf of the dryer. Achieving this uniformity makes it possible to adjust the residence time of the particles on the shelves, taking into account their physical and chemical properties. Any uneven contact of the drying agent with the dispersed material can lead to underheating (with insufficient drying) or overheating with undesirable destruction of particles and reducing its consumer qualities.

The distribution of the gas flow in the working space of the gravitational shelf dryer at different initial velocities in the drying agent inlet is shown in fig. 17.

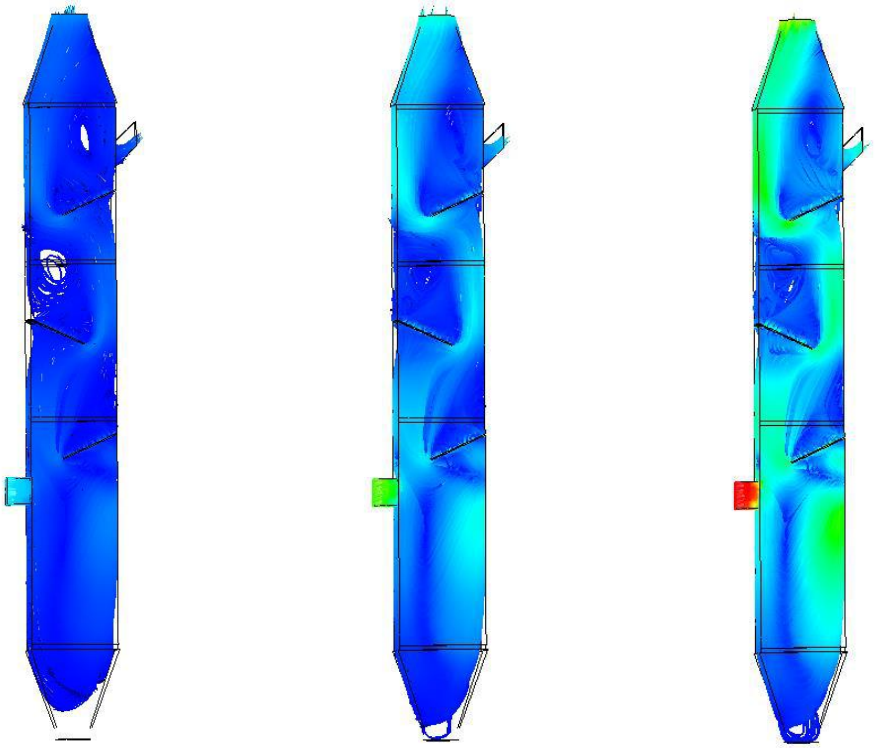

a b c

Figure 17 – The distribution of the gas flow in the working space of the gravitational shelf dryer: a – V=3 m/s; b – V=8 m/s; c – V=15 m/s

The nature of the distribution of the gas flow rate at the stage of the shelf dryer under other conditions of experimental studies (design of the shelf and the flow of gas flow) does not change qualitatively. Peculiarities of the gas flow velocity field distribution depending on the initial conditions of the experiment are given below.

Analysis of the results of the experiment on the distribution of the speed of the gas flow at different stages of the dryer depending on the height of their installation with the same design of each stage showed that:

- the distribution of the velocity of the gas flow becomes more uniform with increasing value of the discharge gap;

Diagram of the gas flow velocity for shelf contact of one structure quantitatively changes its profile. This is due to the redistribution of gas flow in the cross-section of the dryer in height, and with height, it becomes more uniform.

When installing in the volume of the dryer shelf contact with different values of the free cross-section (increase in the free cross-section), the following picture is observed:

- the level of speed of movement of a gas stream on a shelf contact is partially leveled;

- there is a decrease in the peak velocity of the gas flow in the discharge gap;

- plot of the velocity of the gas flow in the transition from the shelf contact to the discharge gap has a smoother character.

Reducing the angle of the shelf contact at a constant value of the gap makes its features in the diagram of the distribution of the velocity of the gas flow:

- there is a decrease in the peak velocity of the gas flow on the shelf, the plot is aligned;

- the peak speed of the gas flow in the discharge gap decreases;

- the zone of the maximum speed of the gas flow in the discharge gap expands with the alignment of the plot.

The diagram of the distribution of the velocity of the gas flow with increasing consumption has the same qualitative law but is characterized by the following distinctive features:

- smoothing of the peak in the middle of the shelf contact;

- equalization of speed along the length of the shelf contact;

- the peak velocity of the gas flow in the discharge gap has a more pronounced character.

Diagrams of the distribution of the gas flow velocity make it possible to determine the zones of gravitational motion of the dispersed material, its soaring in the apparatus, separation, and possible removal. To fully describe the hydrodynamics of the movement of the dispersed material, determine the trajectory of its movement and residence time in the volume of the dryer and the impact on these parameters of the shelf contact design

and gas flow rate, it is necessary to investigate the basic modes of movement of the dispersed material.

It should be taken into account that the design of the shelf and the peculiarities of its location in the working space of the dryer affect the gas flow rate in the overhead space.

This speed is decisive when choosing the mode of movement of dispersed material. The range of existence of the fluidized bed (as it shown in [100-103]) is determined by the first critical velocity $V_{ск1}$ (the gas flow rate that corresponds to the beginning of fluidization) and the second critical velocity $V_{ск2}$ (the gas flow rate that corresponds to the beginning of material removal from the dryer).

As a result of the experiment, as well as on the basis of earlier studies by the authors [104, 105], a general pattern of changes in the nature of the movement of dispersed material on the shelf was obtained (fig. 18).

Each of the modes is characterized by the peculiarities of the movement of dispersed material, as well as the residence time of the material on the shelf, depending on the degree of the constraint of the flow (the relative content of the dispersed phase in the volume of the apparatus) (fig. 19).

The research results allowed us to propose new designs of shelves, which allow providing the required residence time of the material in the dryer (fig. 21).

The use of inclined perforated contact shelves of the above structures allows to creation at each stage of the dryer, such a hydrodynamic situation in which there is an alignment of the plot of the speed of the drying agent along the shelf, its action remains constant in all areas of the shelf. This causes the process of compensation of the action on the dispersed material of inertial forces and rolling on an inclined surface, braking of the dispersed material on an inclined perforated contact shelf, its uniform movement in the suspended layer and long-term contact with the drying agent.

It is possible to implement the proposed constructive solutions (in addition to the design of the dryer, which is shown in fig. 16) in various designs of dryers-classifiers (fig. 22).

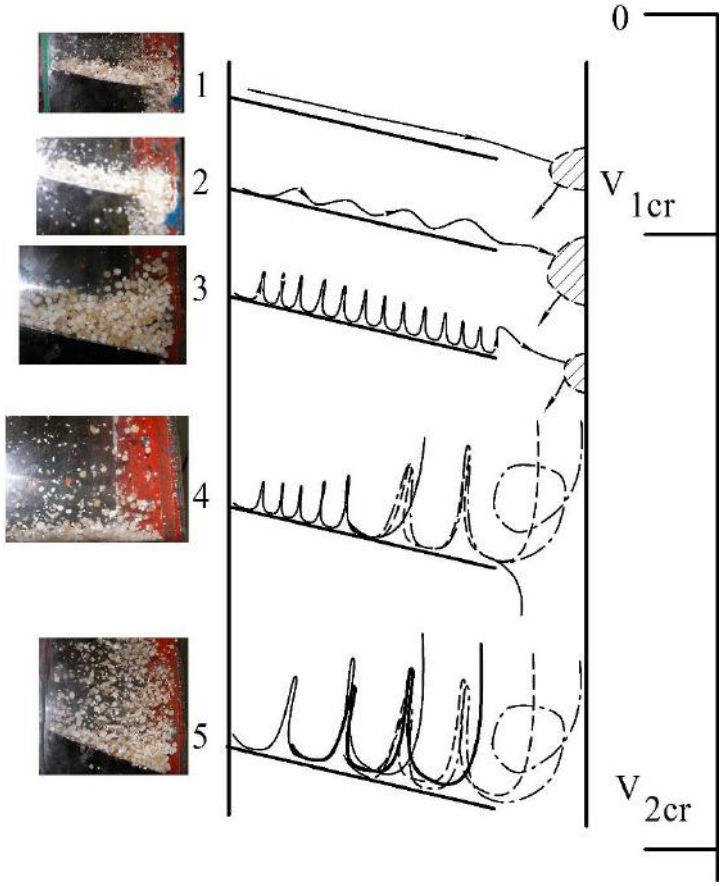

Figure 18 – Operating modes of a multistage gravitational shelf dryer: 1- the gravitational falling layer mode of the dispersed material; 2 - the first transitional mode; 3 - the dryer's operation in the weighted layer mode of the dispersed material; 4 - the second transitional mode; 5 - the dryer's operation in the dispersed material ablation mode

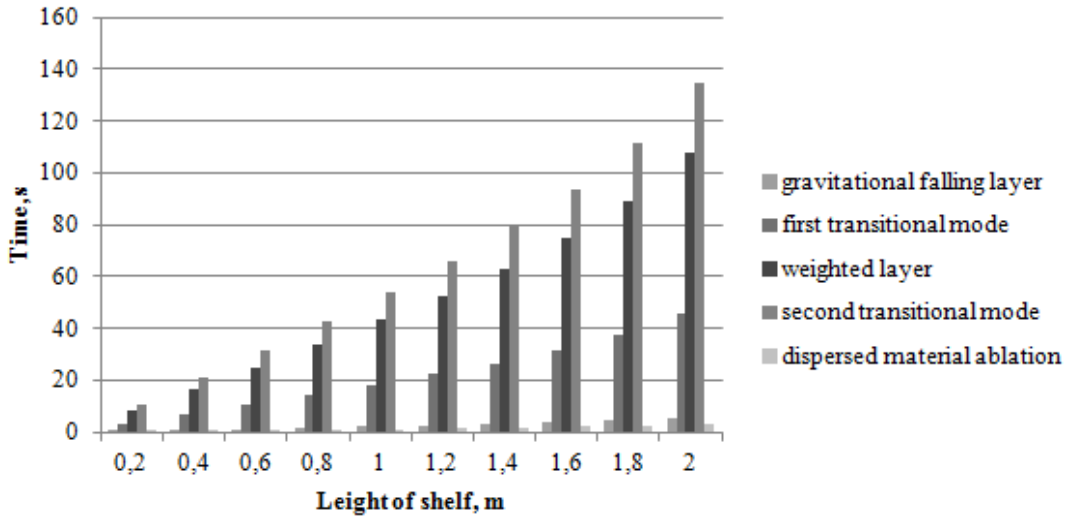

Figure 19 – The residence time of the material on the shelf

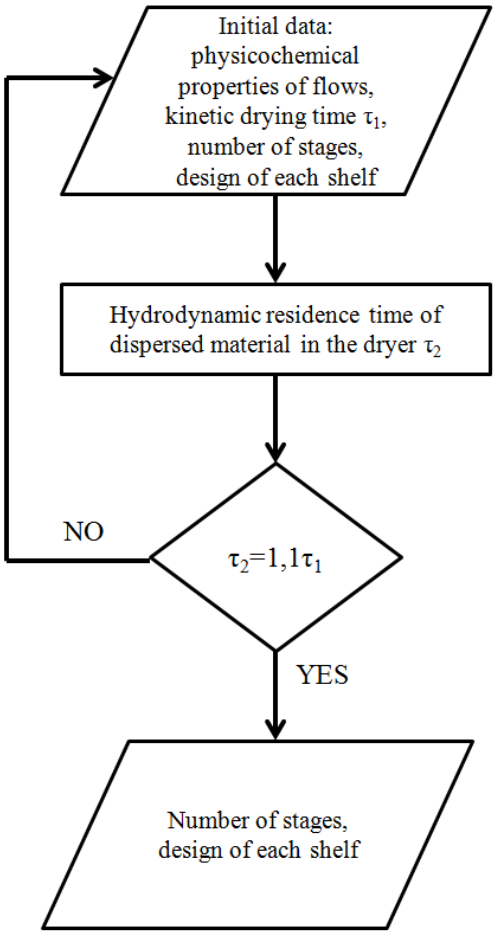

Optimization of the shelves' design, their placement features, and the number of stages in the dryer is carried out according to the criterion of the minimum required "hydrodynamic" residence time of the dispersed material. This time should not exceed by more than 10% the calculated drying time. This approach makes it possible to achieve minimum energy costs and ensure the preservation of the strength (and, in some cases, specific properties, such as, for example, seed germination) properties of the dispersed material.

Based on the obtained results, taking into account studies [106, 107] on the kinetics of moisture removal from dispersed material in devices with an active hydrodynamic regime, an algorithm for engineering calculation of a gravitational shelf dryer is proposed (fig. 20).

It should be noted that the engineering calculation algorithm can be implemented in two ways:

- determination of the design of the dryer, taking into account the provision of the required residence time of dispersed material;
- determination of the design of each stage to ensure the heating time of the dispersed material, the drying time in the constant speed mode and the drying time in the decreasing speed mode.

The second option is more efficient because it allows dividing the dryer into separate zones and a differentiated contact of dispersed material with a drying agent with different temperature and humidity potential is provided.

Figure 20 – Algorithm for engineering calculation of a gravitational shelf dryer (large-block model)

The proposed designs of multistage shelf dryers (in accordance with the model material used in the experiments) can be implemented in industrial drying installations (fig. 23).

One of the most important principles of designing new designs of convective dryers is compliance with energy efficiency requirements because this type of equipment is characterized by sufficiently high values of energy consumption per unit mass of grain product, which is dehydrated. A promising direction to reduce energy costs for creating

a flow of high-temperature drying agent in the apparatus is the development of advanced equipment designs with internal partitioning of the working space using shelf contacts.

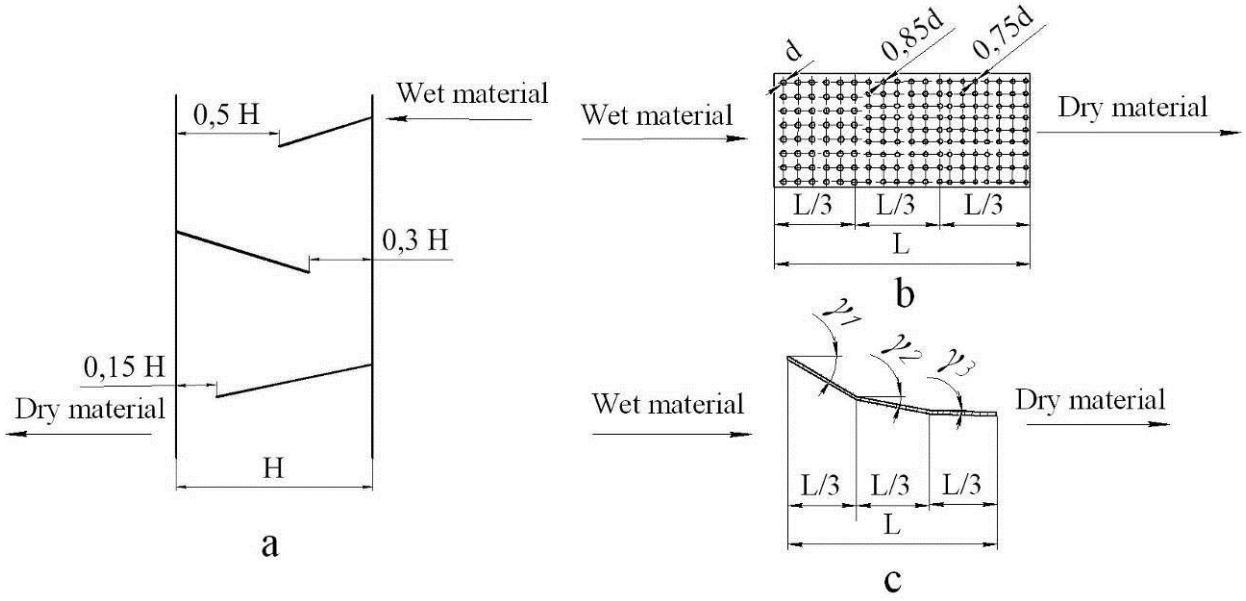

Figure 21 – Constructions of shelves of multilevel gravitational shelf dryer [108-110]: a – shelf with different gap on height of dryer; b – sectioned shelf with variable perforation of sections; c – partitioned sections shelf with constant perforation and variable angle of inclination; d – diameter of hole of perforation; L – length of the shelf; H – width of device; γ_i – angle of inclination of shelf section to horizon.

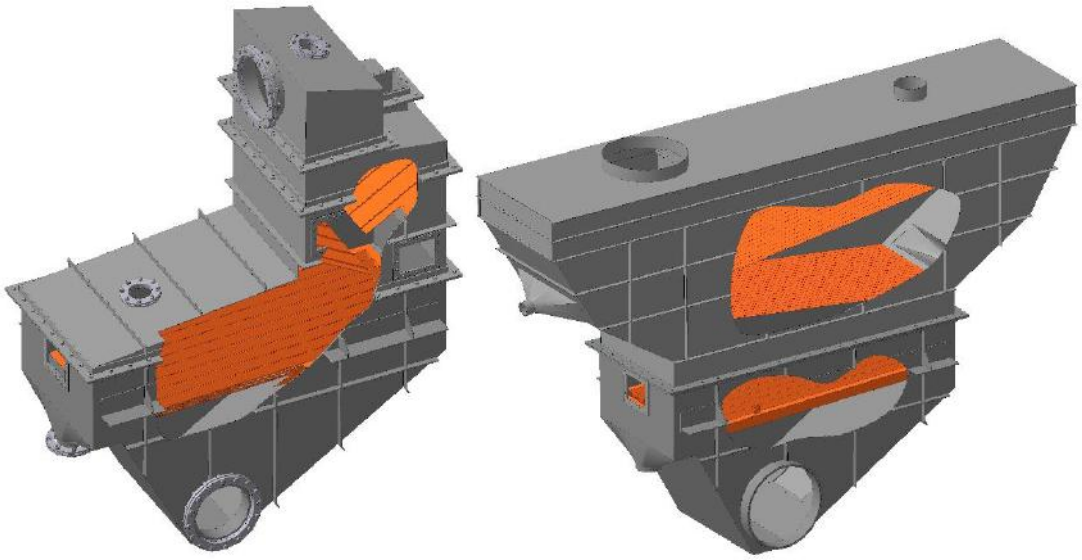

Figure 22 – Constructions of dryers-classifiers

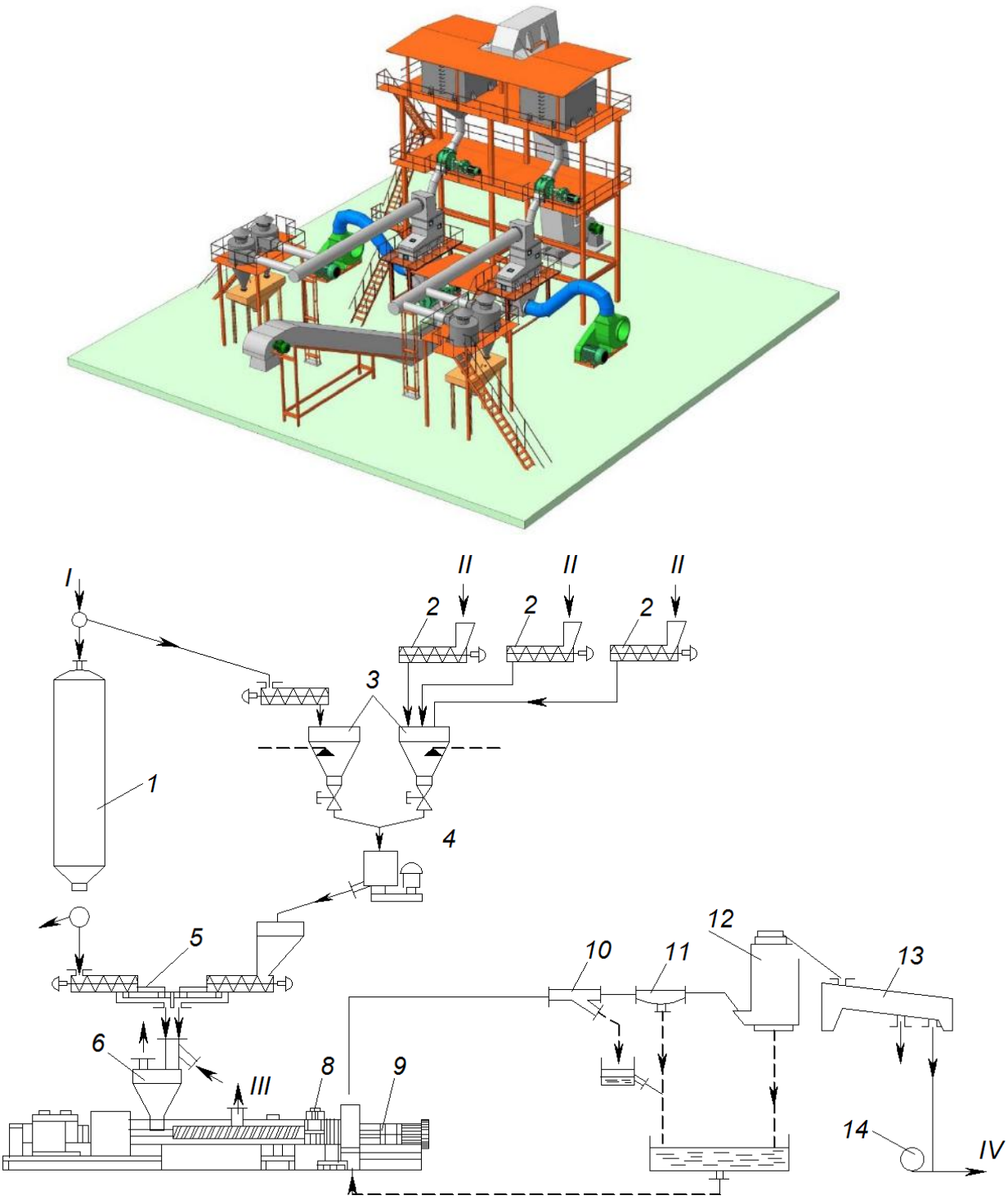

Figure 23 – Technological line of the unit for production of the stabilized and painted polypropylene and polyethylene: 1 – silo for powdered polypropylene; 2 – screw conveyors; 3 – bucket batchers; 4 – high-speed mixer; 5 – the tape batcher; 6 – bunker; 7 – extruder; 8 – the starting valve; 9 – granulator; 10 – damper; 11 – water separator; 12 – dryer; 13 – vibrating sieve; 14 – pneumatic transport; I – polypropylene; II – supplements; III – waste gases; IV – dried polypropylene

The engineering calculation method of such devices is based on the results of theoretical and experimental studies of hydrodynamic parameters of flow motion and kinetics of dehydration of granular materials.

Based on the results of modeling the kinetics of the drying process of a single granular particle, the required time of its dehydration in the flow of the drying agent with the specified characteristics is determined. The theoretically and experimentally hydrodynamic characteristics of the flow of drying agent and dispersed material allow determining the time of its stay in the apparatus depending on the design of shelf contacts and technological parameters of the process. At the stage of analysis of the laws of the kinetics of the process of dehydration of the dispersed material on the cascade of shelves, the optimal organization of the flow is determined, which will provide the minimum energy costs at the required final humidity of the product.

As a result of optimization calculation of the gravity shelf dryer according to the initial data established by the customer of the industrial equipment, it becomes possible to define its following design characteristics:

- the number of shelf contacts in the dryer;
- the angle of inclination of the shelf contacts to the horizon;
- the size of the gap between the end of the shelf contact and the wall of the dryer (or the length of the shelf contact);
- the area of the free section of the shelf contact.

The design characteristics of shelf contacts at each stage of the dryer may differ due to the physicochemical characteristics and strength of the granular material, its stability under long-term exposure to high-temperature drying agent, as well as minimizing energy consumption for the dehydration process.

4 FLUIDIZED BED IN GRAVITATIONAL SHELF DRYERS: OPTIMIZATION CALCULATION

Implementing a fluidized bed in heat-mass transfer processes has become widespread due to the undoubted advantages of such a hydrodynamic system [111-113]. At the same time, there are often difficulties in devices with a fluidized bed providing the required hydrodynamic regime. In this regime, the dispersed phase is predicted to spend in the device the estimated time needed to complete the process. In this case, a significant advantage of devices with a fluidized bed is the ability to control the residence time of the dispersed phase in the workspace of the device [114]. Despite the variety of granulation and drying devices (an overview of methods for obtaining granulated dispersed materials is given, for example, in [115-122]) multistage devices with vertical sectioning of the working space did not receive a wide distribution for drying. The effectiveness of such devices has been proven by the example of various classifiers and granular devices [123-128], which confirms the relevance of their further implementation in the drying technology. The authors of this work attempted a theoretical description [129], experimental studies of the fluidized bed configuration [130], and the conditions for the implementation of heat-mass transfer processes [131] in other devices with the directed motion of the dispersed phase - vortex granulators [132].

The device and principle of a multistage gravitational shelf dryer’s operation can be found in the following studies [133].

The article aims to form an algorithm for calculating the hydrodynamic parameters of the flow in devices with inclined shelves for the implementation of heat treatment and dehydration processes. The research results will complement the general algorithm for the engineering calculation of shelf units, which authors begin to study in the research [134].

The authors use the hypothesis of the possibility to control the motion trajectory and the residence time of the dispersed phase in the dryer's workspace thanks to its directed transfer mechanisms (as shown in the work [135]). The joint solution of the basic

equations of flow motion hydrodynamics, the kinetics of change of the temperature-humidity features in the interacting flows, and the growth rates of granules will allow inventing a rational design of the workspace, heat transfer agent's optimum flow rate and its temperature-humidity features in a shelf dryer. The calculation is carried out by the optimization criterion of the “minimum” hydrodynamic “residence time of the dispersed phase in the workspace of the device”.

Hydrodynamic” time should be equal to “kinetic” time - the period during which the temperature and moisture content features of the dispersed phase should acquire a normative value. This paper presents an algorithm for calculating the "hydrodynamic" residence time of dispersed particles in a shelf dryer's working space. At the same time, the drying operating temperature was maintained in the dryer, which, for example, for granules of porous ammonium nitrate was 105-110 °C.

There are multiphase flows of different nature. Their survey is observed, for example, in [136-138] for various processes. The following types of multiphase flows should be distinguished. In the first case, the considered volume is filled with the substance of one phase. The sub-stance of another phase occurs in the form of discrete particles (solid phase) or bubbles (gaseous phase) where the volume rate of the substance of the other phase is low (up to 10% of the total volume). In the second case, the considered volume is partially filled with liquid and partly with gas, which does not mix and the free surface separates them from each other. In the most difficult case, substances of different phases can mix (dissolve / stand out from solution), and the volume rate of the substance of another phase is large (over 10 % of the total volume). Various approaches are used to model these multiphase flows.

In many cases, it is possible to use the dispersed particles model, the mixing model, and the multiphase Euler model, to simulate flows in which substances of different phases can mix and do not form a free surface. Additional criteria for choosing a model include [138].

The ratio β of substance mass of the dispersed phase (*df*) to the substance mass of the carrier phase (*cf*) [139]:

$$\beta = \psi \frac{V_{df}}{V_{cf}}, \quad (45)$$

where V_{df} and V_{cf} are the volume of the dispersed and carrier phases,

ψ is the ratio of the dispersed and carrier phases density,

$\psi = \rho_{df}/\rho_{cf}$; ρ_{df} – dispersed phase density;

ρ_{cf} - carrier phase density; this ratio can be over 1000 for solids in a gas flow, about 1 for solids in a liquid flow, and less than 0.001 for gas particles in a liquid flow [139].

At a low β ratio, dispersed particles practically do not affect the carrier phase flow, and any of the listed models can be used [139]. At very remarkably values of β, dispersed particles strongly affect the carrier phase flow, and only the multiphase Euler model should be used for the proper simulation of the flow. With average β values, one needs to calculate the Stokes number to select a suitable model, as described below.

Stokes number St [140]:

$$St = \frac{\tau_{df}}{\tau_{cf}}, \quad (46)$$

where τ_{df} is the time describing the motion of particles, $\tau_{df} = (\rho_{df} d^2)/(18 \mu_{cf})$,

d is the particle diameter,

μ_{cf} is the viscosity of the carrier phase,

$\tau_{cf} = l_{cf}/u_{cf}$ is the time describing the carrier phase flow,

l_{cf} is the peculiar length,

u_{cf} is the peculiar velocity.

If $St << 1.0$, the dispersed phase particles almost do not deviate from the streamlines of the carrier phase, and any flow model can be used (as a rule, the mixing model is the least resource-intensive) [141]. If $St > 1.0$, the trajectory of the dispersed phase particles completely does not coincide with the carrier phase streamlines, and the mixing model is unsuitable in this case: either the dispersed particles model or the multiphase Euler model must be used [141].

In the case under consideration, the dispersed phase motion trajectory applies to the dispersed particle model. The substance forming the main phase is assumed to be a continuous space, and its flow is modeled (depending on the flow turbulence degree) by the Navier – Stokes or Reynolds equations and the flow continuity. The substance in the flow in the form of discrete particles does not form a continuous medium. Individual particles interact with the flow of the main phase and with each other discretely. The Lagrange approach is used to model the motion of the particles of the dispersed phase. It means that the motion of the separate particles of the dispersed phase influenced by forces from the side of the main phase flow, is controlled.

It should be noted that there is a constrained motion of particles (discrete particles, a solid phase, occupies a volume greater than 10 % of the total space in the device) in the industrial model of a shelf dryer. In this case, the calculation model should be supplemented with a block that allows defining how the particles' residence time changes (increases) in the dryer if the volume of particles increases more than 10 % [139].

The fraction composition of particles (distribution by size), the motion of which is modeled in this work is shown in Fig. 24.

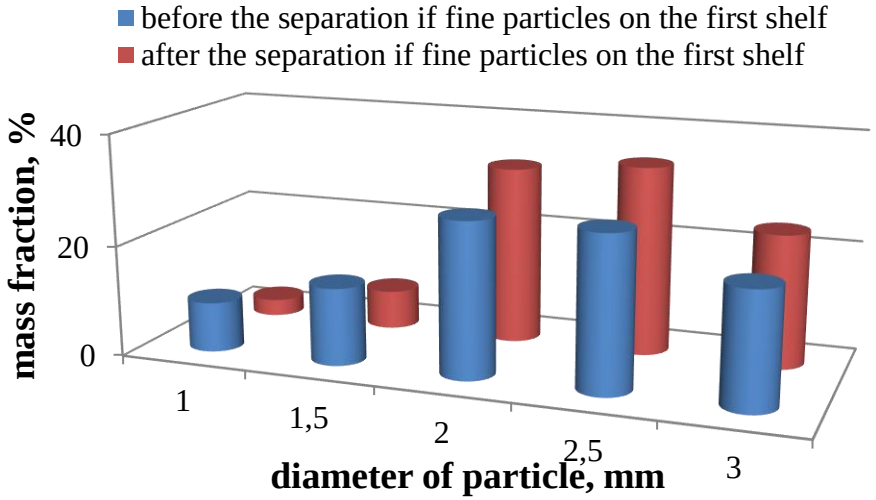

Figure 24 – The fraction composition of particles

The previous experimental studies [132] demonstrate that the gas flow in the shelf dryer is turbulent. Direct modelling of the turbulent flows by calculation of the Navier –

Stokes equations written for instantaneous velocities is complicated. Besides, not instantaneous, but time-averaged velocity values attract attention. For the analysis of turbulent flows, the Reynolds equation and the continuity of the flow are used [112, 136]:

$$\frac{\partial}{\partial \tau}\left(\rho_{cf}\overline{u_{cfi}}\right)+\frac{\partial}{\partial x_j}\left(\rho_{cf}\overline{u_{cfi}u_{cfj}}\right)+\frac{\partial}{\partial x_j}\left(\rho_{cf}\overline{u'_{cfi}u'_{cfj}}\right)=-\frac{\partial p}{\partial x_i}+\frac{\partial}{\partial x_j}\left[\mu_{cf}\left(\frac{\partial \overline{u_{cfi}}}{\partial x_j}+\frac{\partial \overline{u_{cfj}}}{\partial x_i}\right)\right]+f_i,' \tag{47}$$

$$\frac{\partial \rho_{cf}}{\partial \tau}+\frac{\partial}{\partial x_j}\left(\rho_{cf}u_{cfj}\right)=0, \tag{48}$$

where $\overline{u_{cf1}}$, $\overline{u_{cf2}}$, $\overline{u_{cf3}}$ – time-averaged velocities of carrier phase,

$\overline{u'_{cf1}}$, $\overline{u'_{cf2}}$, $\overline{u'_{cf3}}$ – pulsation component of velocities of carrier phase.

In equations (47) and (48) the simplified equations are used, i, j = 1… 3, the summing up to over the same indices are assumed, x_1, x_2, x_3 - coordinate axes, τ - time. The f_i term expresses the action of mass forces.

In this system of 48 equations, the independent sought parameters are 3 velocity components u_{cf1}, u_{cf2}, u_{cf3} and pressure p. The density ρ_{cf} of the gas, at velocities up to about 0.3 of the Mach number, can be assumed to be constant.

As the boundary conditions, the adhesion condition is set on all solid walls (the velocity is zero), the distribution of all velocity components in the inlet section, and the first derivatives (in the direction of flow) of the velocity components in the outlet section are equal to zero. Besides, the direct interest is the distribution of the velocity along the length of the device in space above the shelf, where the motion of dispersed particles occurs.

The range of existence of a fluidized bed in a shelf device is limited by such two boundary conditions or two critical gas flow (carrier phase) velocities: (i) the first critical velocity or the velocity of the start of fluidization; (ii) the second critical velocity or the velocity of the start of ablation. The values of these velocities depend on the size (diameter) of the dispersed phase, the flow rate of the carrier phase, and the velocity in

the overhead space of the device (depends on the value of the free section of the shelf, its tilt angle, length, etc.).

Let us assume that the dispersed phase particles have a spherical shape. The forces influencing this particle are caused by the difference between the particle velocity and the flow velocity in the main phase and the displacement of the main phase by this particle. The equation regarding the motion of such a spherical particle is as follows [137]:

$$m_{df}\frac{du_{df}}{d\tau}=3\pi\mu_{df}dC_{cor}\left(u_{cf}-u_{df}\right)+\frac{\pi d^3\rho_{cf}}{6}\frac{du_{cf}}{d\tau}+\frac{\pi d^3\rho_{cf}}{12}\left(\frac{du_{cf}}{d\tau}-\frac{du_{df}}{d\tau}\right)+F_e \qquad (49)$$

Here m_{df} - the mass of the particle,

d - the diameter of the particle,

u_{df}, u_{cf} - velocity;

ρ_{df}, ρ_{cf} - density;

μ_{df} - the dynamic viscosity of the substance in the main phase,

C_{cor} - its viscous resistance coefficient;

F_e - an external force which is directly acting on a particle (for example, gravity, aerodynamic drag, centrifugal force etc.);

index *df* refers to the dispersed phase, index *cf* refers to the carrier phase.

According to Stokes's law, the first term on the right-hand side of equation (49) expresses the deceleration of the particle as a result of viscous friction against the flow of the main phase. The second term is the force applied to the particle due to the pressure drop in the main phase surrounding the particle caused by the main phase flow's acceleration. The third term is the force required to accelerate the main phase's weight in the volume displaced by the particle.

The detailed description of this model is described in work [136] in applying three-phase vortex separators.

Let us consider the motion of a particle in the inter-shelf space. At air velocity $u_{cf} > u_{cr1}$ in the shelf space (u_{cr1} - the first critical velocity or the velocity of the start of

fluidization), it will be in a weighted state until it reaches $u_{cf} = u_{cr2}$, causing the ablation (u_{cr2} - the second critical velocity or the velocity of the start of ablation). If the air velocity is $u_{cf} < u_{cr2}$, then this difference of velocities $\Delta u_{cf} = u_{cr2} - u_{cf}$ will make the particle to move from top to bottom. If $u_{cf} < u_{cr1}$, the particle will move in the gravitational falling layer mode with a sharp decrease in the residence time on the shelf. Given that the gas flow transmits up to 95 % of the momentum of the dispersed material, we suppose that the difference in particle velocities Δu_{df} will be approximately equal to the difference of velocities Δu_{cf} ($u_{df} \approx u_{cf}$; $\Delta u_{df} = u_{cr2} - u_{df}$).

The time of the particle motion the along the shelf with the tilt angle $\gamma = 90°$ and the length L_s on the i-th stage of the shelf device will be equal to:

$$\tau_i = \frac{L_s}{\Delta u_{df}} \approx \frac{L_s}{\Delta u_{cf}} \tag{50}$$

In the case when the tilt angle of the shelf is small (in practice within 10–35°), the velocity Δu_{df} that describes the motion of the particle from top to bottom, will actually have one roll down component $\Delta u_{df} \cdot \sin\gamma$, because the normal force of particle pressure on the shelf and, accordingly, normal acceleration components and velocities $\Delta u_{df} \cdot \cos\gamma$ will be compensated by the normal reaction of the shelf.

Thus, the motion time of the particle τ_i along the shelf on the *i-th* stage is calculated by the equation:

$$\tau_i = \frac{L_s}{\Delta u_{df} \sin\gamma} \tag{51}$$

which is simplified with $\gamma = 90°$ to the previous expression (50).

Obviously, the ratio of the particle's motion time along the shelf is inversely proportional to the sines of the tilt angle γ of the shelf:

$$\frac{\tau_1}{\tau_2} = \frac{\sin\gamma_2}{\sin\gamma_1} \tag{52}$$

According to these considerations, it is possible to define the possible constructive influence on the residence time of the particle in the inter-shelf space and the regulation of the drying process. The residence time of the dispersed particle (drying time) at this stage is increased by reducing the tilt angle of the shelf.

Formula (51) allows defining the residence time of a particle on the shelf that moves independently of other particles, i.e. its free motion is considered. Such free motion is observed only at small volumetric contents of the dispersed phase in a two-phase system, when there is such a distance between the particles where collisions or mutual influence of the particles are absent. If $\delta \geq 0.1$ (constrained particle motion), there are some changes in the system: the distances between the particles' surfaces or the size of the passages between the particles become smaller than their diameter, and the particle cannot slip freely between the other two particles [143]. It is necessary to consider the collision effect of particles with each other. Besides, the collision of particles in a two-phase system can also occur when the dispersed phase consists of polydisperse particles or particles with different densities.

It is possible to consider the limited particle motion phenomenon and the interphase interaction force when introducing the constraint coefficient of the particle χ.

Various formulas are obtained to identify the particles constraint coefficient, based on different schemes of the dispersed phase particles location. In particular, the following formula considers the scheme with random free filling [144]:

$$\chi = (1-\delta)^{-n}, \tag{53}$$

where δ - coefficient of constrained particle motion that takes into account the type of filling material;

δ = 0.6 (the case of random free filling [143]);

n - exponent that takes into account the constraint of the material flow; n = 3–5 (accepted as preliminary data and should be specified by the experimental studies and computer modelling).

Thus, expression (51) will be as follows:

$$\tau_i = \frac{L_{sh} \cdot \chi}{\Delta u_{cf} \cdot \sin\gamma}. \quad (54)$$

The results from hydrodynamic indices calculations in the shelf dryer are presented by two blocks: the velocity of the gas flow over the dryer's shelf and the residence time of particles in the device in constrained motion.

Let us consider the dependence of the ascending velocities profile on the structural features of the inter-shelf space, namely, the length of the shelves, the degree of their perforation and the installation angle γ. The ascending velocities profile will have a peculiar peak in the inter-shelf space with no perforation (Fig. 25).

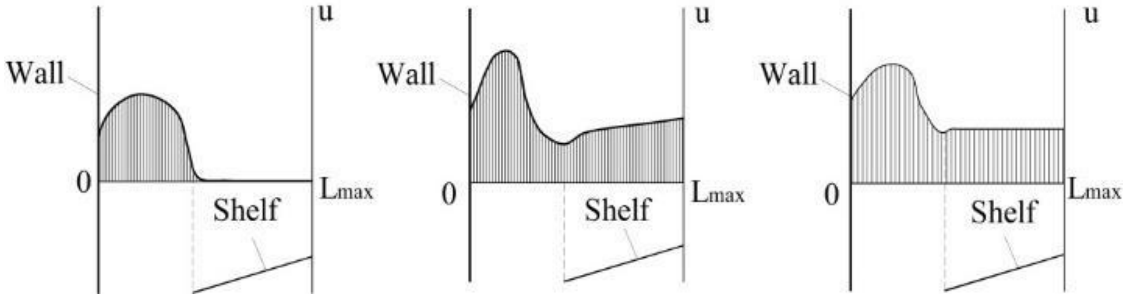

Figure 25 – Gas flow velocity profiles: a – non-perforated shelf; b – perforated shelf with constant length perforation; c – perforated shelf with variable length perforation

In the presence of perforation, the peak decreases according to the increase in the drying agent's flow rate through the sectioning shelves holes (Fig. 24 b). Optimization of the ascending velocity profile can be achieved not only by changing the outloading gap and the tilt angle of the shelves, but also by varying the perforation degree along the shelves (Fig. 24 c).

When establishing shelf contacts with different outloading gap, the epure of the gas flow velocity distribution has the following features:

- the distribution of the gas flow velocity has the descending nature from the wall of the device to the end of the shelf contact. It is caused by the length difference of the pressure under the shelf contact and above it;

- when reducing the ratio of the current length to the length of the shelf *X/L*, starting from the middle of the shelf contact, there is an intense decrease in the gas flow velocity, caused by the creation of swirls in the outloading gap. Reducing the outloading gap size leads to an increase in the intensity of swirls at the end of the shelf contact, which disrupts the ascending motion of the gas flow;

- the minimum velocity value of the gas flow at the shelf contact is greater, the smaller the outloading gap value is.

The results analysis regarding the gas flow velocity distribution at different stages of the dryer depending on their height with the same design of each stage showed that:

- the distribution of the gas flow velocity becomes more uniform with the increasing value of the outloading gap;

- the epure of the gas flow velocity for shelf contact of one structure quantitatively changes its profile. It is caused by the gas flow redistribution in the dryer's cross section in height, and with the height it becomes more uniformed.

When installing shelf contact with different values of the free cross-section (the free cross-section increase) in the dryer, the following situation is observed:

- the level of the gas flow motion velocity is partially leveled on a shelf contact;

- there is a decrease in the peak velocity of the gas flow in the outloading gap;

- the epure of the gas flow velocity in the transition from the shelf contact to the outloading gap has a smoother character.

Reduction of the shelf contact angle at a constant gap *X/L* puts its features in the epure of the gas flow velocity distribution:

- there is a decrease in the peak velocity of the gas flow on the shelf, the epure is leveled;

- the peak velocity of the gas flow decreases in the outloading gap;

- the zone of the gas flow maximum velocity in the outloading gap is expanded with the alignment of the epure.

The epure of the gas flow velocity distribution with increasing consumption has the same qualitative law, but is characterized by the following distinctive features:

- smoothing of the peak in the middle of the shelf contact;

- leveling of the velocity along the length of the shelf contact;

- the peak velocity of the gas flow in the outloading gap is more expressed.

Epures of the gas flow velocity distribution enable to define the gravitational motion zones of the dispersed material, its soaring in the device, separation, and possible ablation. It is necessary to investigate the basic modes of the dispersed material motion to describe the hydrodynamics of the dispersed material motion, identify its motion trajectory and residence time in the dryer and the impact on these parameters of the shelf contact construction and gas flow rate.

Analysis of the previous studies in the two-phase flows modelling field, which consist of gas as a dispersion phase and dispersed particles, shows that one of the most promising ways to calculate the motion of particles is the so-called trajectory method [145-147]. The authors [148,149] conclude that in modelling, the constrained motion of particles with large (0.5–5 mm) diameter can be based on the Lagrangian model of force analysis of particle motion using differential equations of motion which have already been used to describe hydrodynamic conditions of dispersion phases in the workspace of the shelf device. At the same time, for the case of granules motion in the workspace of the device, the application of the trajectory method is complicated by the following:

- polydispersity of the system;

- constrained motion of granules in the shelf device.

Thus, the trajectory method with highly accurate results can be used only if there is a software that allows one to export a theoretical model of the single particle motion and to take into account the degree of flow constraint.

In this work, the software product Ansys Fluent is used to export the original mathematical model, to calculate the granules trajectories and the distribution law of the polydisperse system in the workspace of the shelf device taking into account the concentration of the dispersed phase (the flow constraint).

Results visualization of the polydisperse system motion modelling in Fig. 26 (relative content of the dispersed phase in the workspace $\psi = 0.2$).

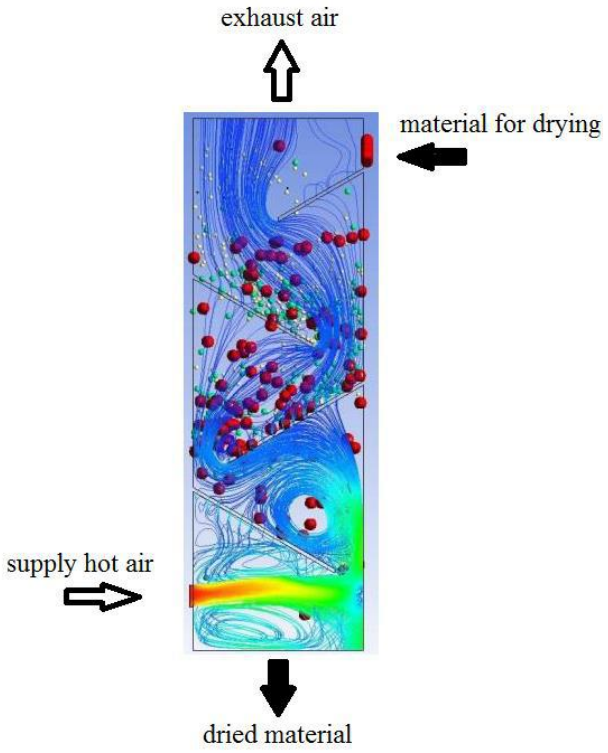

Figure 26 – Visualization of results of the poly disperse system constrained motion modelling in the shelf device

The methodology for carrying out this stage in the research allows inserting the calculated number of granules of a certain size as initial data (analog of the polydisperse system's fractional composition) and the total number of granules (analog of the degree of dispersed flow compression). With the help of this technique it becomes possible to define the dispersed phase trajectories and refine the empirical constraint coefficient m to calculate the constrained motion time.

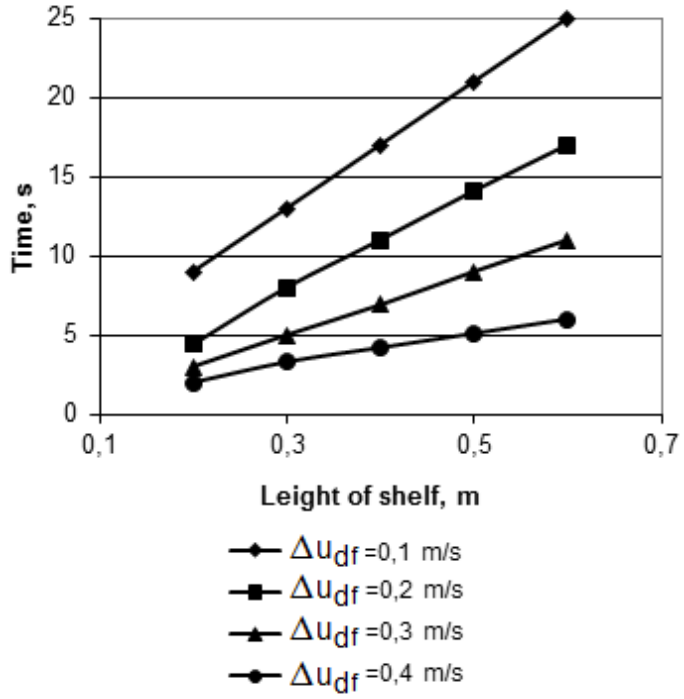

Figure 27 – The residence time of the particle on the shelf (free motion): d_p = 2 mm; ψ = 25 %, $\gamma = \gamma_0 + (11–13)^o$

Figs 27–30 show data for calculating the residence time of dispersed material on the shelf in free and constrained mode, and an example of comparing data for determining the residence time of dispersed material in the constrained mode according to the theoretical model, experimental data and computer modelling data.

Data from Fig. 26 show that the results of computer modelling give a higher value of the residence time of the dispersed phase on the shelf in the device. It is explained by the inhibition of particles not only due to the action of neighboring particles, but also due to the creation of a vortex gas flow zone at the end of the shelf.

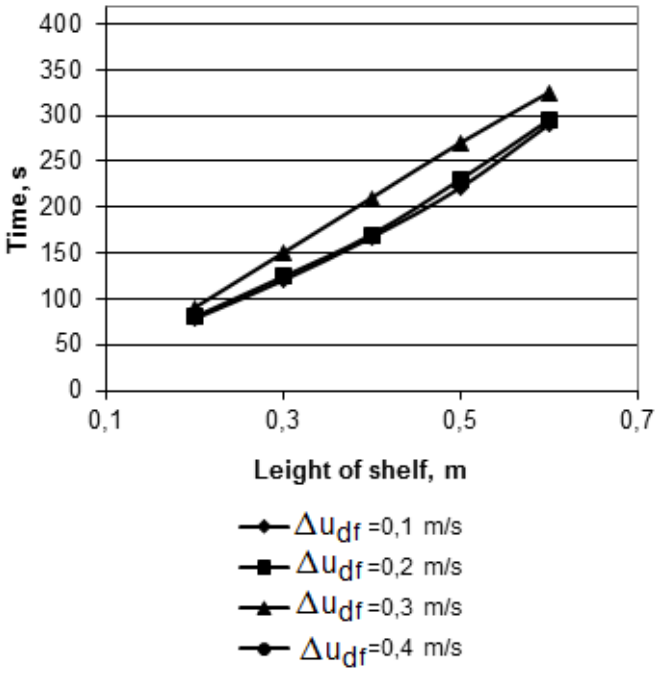

Figure 28 – The residence time of the particle on the shelf (constrained motion): dp = 2 mm; ψ = 25 %, γ = γ0 + (11–13)º, δ = 0.6

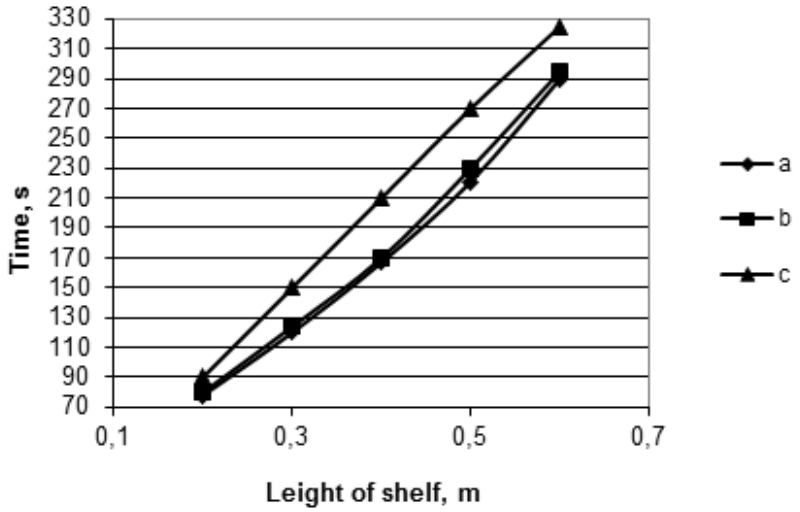

Figure 29 – The residence time of the particle on the shelf (constrained motion): d_p = 2 mm; ψ = 25 %, $\gamma = \gamma_0 + (11–13)^\circ$, δ = 0.6, Δu_f = 0.2 m/s; a – data from the theoretical calculation; b – data of the experimental studies; c – data of the computer modelling

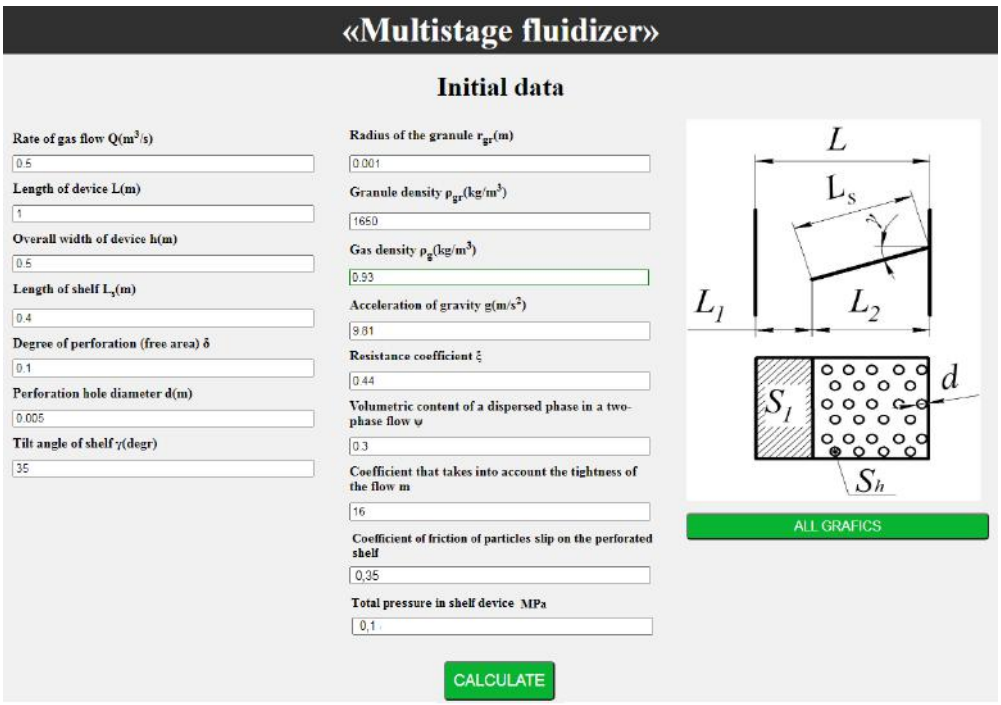

Figure 30 – The software "Multistage fluidizer"©: the main window

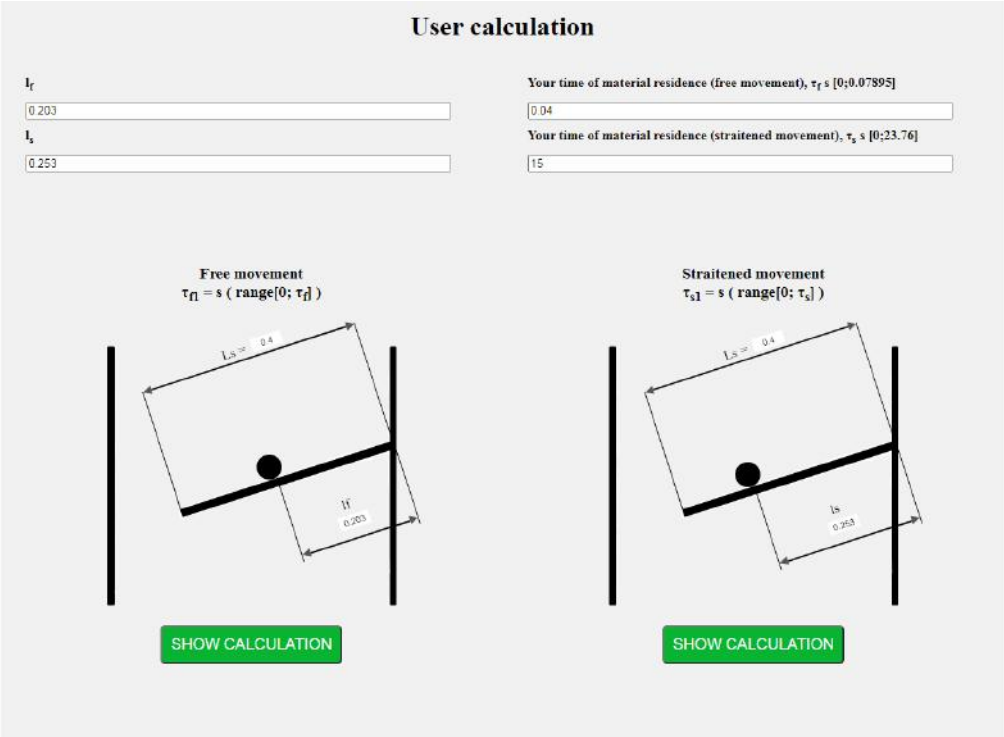

Figure 31 – The software "Multistage fluidizer"©: the main window

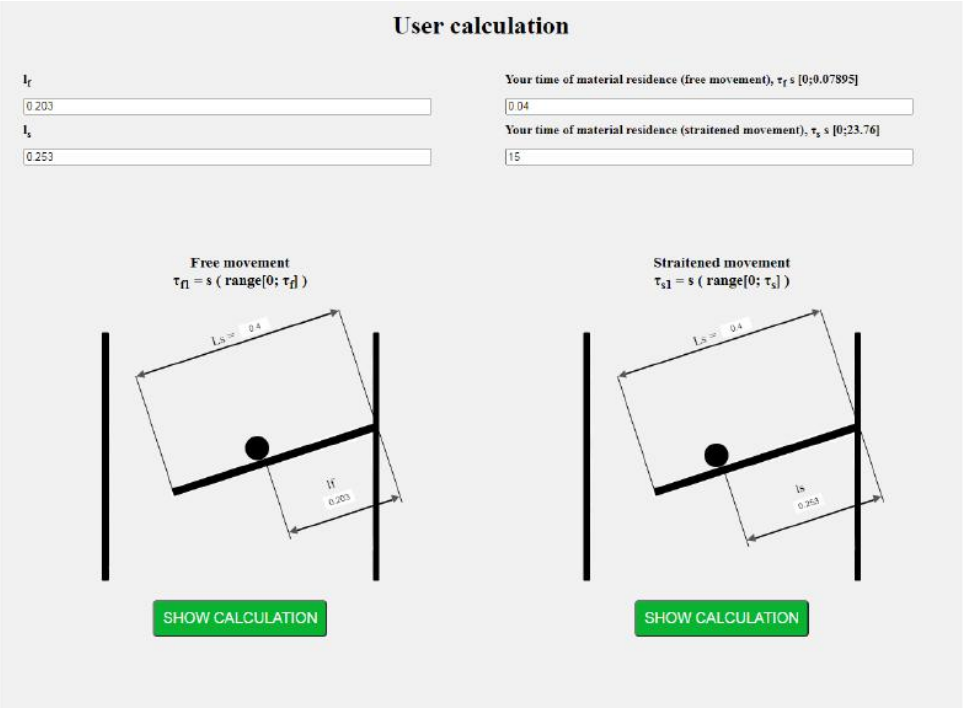

Figure 32 – The software "Multistage fluidizer"©: results of calculation

Based on the results of the experimental research data analysis and computer modelling, the value of the exponent m in formula (53) was refined. The experimental range of the exponent, as can be seen from the graph shown in Fig. 27, differs little from the theoretical ones. However, in this work it is recommended to use the indicator m, which is obtained from computer modelling, considering the peculiarities of the hydrodynamic picture at the end of the shelf. A narrower value of n = 5.4–5.7 is proposed.

The research results the creation of the software "Multistage fluidizer©" [150], which calculates the residence time of the material on the dryer's shelf, depending on its construction and features of the gas flow. The interface of the software and the results of some calculations are shown in Figs 30, 31. For the first time this software was presented by the authors in the work [151]. In this article, the software has been improved in terms of calculating the residence time of particles in a shelf unit in a constrained mode. The values of the coefficients that are given in the program are taken on the basis of the literature data [112, 134].

The software makes it possible to predict the change in the residence time of dispersed material at the gravity shelf dryer stage and to obtain data on the optimal technical and economic indices of the device in terms of material flow rate for production and energy for creating a fluidized bed of a given configuration.

Also, it is planned to use the neural network [152, 153] for optimization of this calculation for further research:

moisture of the material i-stage of the dryer x (kg of water/kg of material);

moisture of the drying agent in i-stage of the dryer b (kg of water/kg of material).

CONCLUSIONS

This section is prepared in according to data [1-4].

Due to the creation of an active hydrodynamic mode to weigh solid particles in a layer, a multistage fluidized bed device with inclined perforated shelves provides efficiency to carry out heat-mass transfer processes.

Changes in the constructive parameters of the inclined shelf (the width of the outloading space and the shelf perforation degree) identify the different nature of the gas flow distribution between the holes of the shelf and the outloading space.

Various hydrodynamic modes during operation of the device were revealed: the “gravitationally falling layer” mode and the “weighted layer” mode. The first mode is effective in carrying out pneumatic classification processes, and the second—in cooling and drying of granular materials.

The study of interphase heat transfer showed a higher intensity of heat transfer in the weighted layer on an inclined perforated shelf compared to a traditional fluidized bed on a horizontal gas distribution grid.

The theoretical model enables to present the gas flow velocity profiles depending on the length and perforation degree of the shelf contact, as well as to estimate the residence time of material particles in the workspace of the device.

Further research will point to develop the mathematical model of the weighted layer hydrodynamics on an inclined perforated shelf. The corresponding scientific and methodological approaches based on using artificial neural networks for parameter identification of the proposed mathematical model will be developed.

The necessity of the final drying stage in the PAN production is proved. An improved scheme for obtaining PAN is shown. Based on the literature data, the authors propose to use a new design of the drying device. The proposed design of a multistage shelf dryer allows being carried out the drying process in a differentiated mode (the contact of the material at each stage is carried out with a drying agent with different

temperature and humidity potential), which creates conditions for controlling the dehydration process and forming a nanoporous structure.

The heating and drying process of PAN granules are described. Dependencies for determining the temperature and humidity features of PAN granules during the drying stage are obtained. The temperature and humidity feature of the material closes the system of heat and mass transfer equations. For drying process calculation in the concentration zones, in this case, it is necessary to know the thermophysical properties of the dispersed material. Moreover, one can use a similar temperature-humidity approximation to define the mass transfer coefficient and mass transfer properties. The material is heated with different intensities at a constant radius of the particle, depending on its thermophysical properties. The particles with similar thermophysical properties are heated more intensely when their radius decreases.

A comparative study regarding the surface morphology of PAN granules is carried out. The main features of the nanoporous structure of the samples after the final drying stage are presented. On the surface, there are twisted and deep nanopores of different sizes. The surface structure of granules is changed toward decreasing the number of cavities and their replacement by deep pores increases tortuosity nanopores, their number and the relative area of the porous surface.

Comparative analysis of the quality indicators of PAN granules using the final drying stage and without it, demonstrates usefulness to introduce the final drying into the PAN production. Behind the realization of the final drying stage in the gravitational shelf dryer, the strength of the granules does not decrease since a new cycle of heat treatment is absent and the granule continues to dry at the same temperature. The indicator of absorptivity index increases because instead of cavities on the granule; the indicator of retentivity index increases because the number of twisting deep micropores increases. The relative value of mechanical pores decreases because the total number of micropores / mesopores / macropores increases. The ratio between micropores / mesopores / macropores changes increasing micropores.

REFERENCES

1. Al Amin, I.; Bińi, A. Application of the fluidized bed process for formulation of WG-type pesticide granules. *Powder Technol.* **1994**, *79*, 135–146, doi:10.1016/0032-5910(94)80008-1.
2. Lipin, A.G.; Nebukin, V.O.; Lipin, A.A. Assessment of coverage degree during particulate material encapsulation in fluidized bed. *Izv. Vyss. Uchebnykh Zaved. Khimiya Khimicheskaya Tekhnol.* **2019**, *62*, 84–90, doi:10.6060/ivkkt201962fp.5793.
3. Li, Z.; Kind, M.; Gruenewald, G. Modeling Fluid Dynamics and Growth Kinetics in Fluidized Bed Spray Granulation. *J. Comput. Multiph. Flows* **2010**, *2*, 235–248, doi:10.1260/1757-482X.2.4.235.
4. Ostroha, R.; Yukhymenko, M.; Yakushko, S.; Artyukhov, A.E. Investigation of the kinetic laws affecting the organic suspension granulation in the fluidized bed. *East. Eur. J. Enterp. Technol.* **2017**, *4*, 4–10, doi:10.15587/1729-4061.2017.107169.
5. Pusapati, R.T.; Rao, T.V. Fluidized bed processing: A review. *Indian J. Res. Pharm. Biotechnol.* **2014**, *2*, 1360–1365.
6. Kornienko, Y.; Hayday, S.; Liubeka, A.; Martynyuk, O. Kinetic laws of the process of obtaining complex humic-organic-mineral fertilizers in the fluidized bed granulator. *Ukr. Food J.* **2016**, *5*, 144–154.
7. Si, C.; Wu, J.; Wang, Y.; Zhang, Y.; Shang, X. Drying of low-rank coals: A review of fluidized bed technologies. *Dry. Technol.* **2015**, *33*, 277–287, doi:10.1080/07373937.2014.952382.
8. Sizgek, E.; Sizgek, G.D. Drying Characteristic of *Porous ceramic* microspheres in a microwave heated fluidised bed. *Chem. Eng. Technol.* **2002**, *25*, 287–292, doi:10.1002/1521-4125(200203)25:33.0.co;2-l.
9. Randel, E.; Schak, J.; Islam, A. Fluid-bed dryers: static versus vibrating. *GEA Process Eng.* **2013**, April, 1–7.
10. Zhang, Y.; Zhao, Y.; Dong, L.; Duan, C.; Zhou, E.; Lu, J.; Zhang, B.; Yang, X. Flow pattern transition characteristics in vibrated gas-solid fluidized bed of Geldart B

magnetite powder using pressure drop signals analysis. *Powder Technol.* **2018**, *327*, 358–367, doi:10.1016/j.powtec.2017.12.089.

11. Zeilstra, C.; Van Der Hoef, M.A.; Kuipers, J.H. Experimental and numerical study of solids circulation in gas-vibro fluidized beds. *Powder Technol.* **2013**, *248*, 153–160, doi:10.1016/j.powtec.2013.03.045.
12. Jin, H.; Zhang, J.; Zhang, B. The effect of vibration on bed voidage behaviors in fluidized beds with large particles. *Braz. J. Chem. Eng.* **2007**, *24*, 389–397, doi:10.1590/s0104-66322007000300008.
13. Singh, R.I.; Ghule, K. Design, development, experimental and CFD analysis of a prototype fluidized bed stripper ash cooler. *Appl. Therm. Eng.* **2016**, *107*, 1077–1090, doi:10.1016/j.applthermaleng.2016.07.044.
14. Rogala, Z.; Kolasiński, P.; Gnutek, Z. Effect of operating conditions on performance of silica gel-water air-fluidised desiccant cooler. In Proceedings of the International Conference on Advances in Energy Systems and Environmental Engineering (ASEE), E3S Web of Conferences, EDP Sciences, Wrocław, Poland, 7 November 2017; p. 146.
15. Rogala, Z.; Kolasiński, P.; Błasiak, P. The influence of operating parameters on adsorption/desorption characteristics and performance of the fluidised desiccant cooler. *Energies* **2018**, *11*, 1597, doi:10.3390/en11061597.
16. Katz, V. Cooling of granules in vibrating, suspended bed: Engineering simulation. *Mod. Mech. Eng.* **2016**, *6*, 76–90, doi:10.4236/mme.2016.62009.
17. Zhang, Y.M.; Lu, C.X.; Shi, M.X. A practical method to estimate the bed height of a fluidized bed of fine particles. *Chem. Eng. Technol.* **2008**, *31*, 1735–1742, doi:10.1002/ceat.200800351.
18. Hu, X.; Calo, J.M. Plastic particle separation via liquid-fluidized bed classification. *AIChE J.* **2006**, *52*, 1333–1342, doi:10.1002/aic.10721.
19. Azimi, E.; Karimipour, S.; Xu, Z.; Szymanski, J.; Gupta, R. Statistical analysis of coal beneficiation performance in a continuous air dense medium fluidized bed separator. *Int. J. Coal Prep. Util.* **2015**, *37*, 12–32, doi:10.1080/19392699.2015.1123155.

20. He, J.; Zhao, Y.; Zhao, J.; Luo, Z.; Duan, C.; He, Y. Enhancing fluidization stability and improving separation performance of fine lignite with vibrated gas-solid fluidized bed. *Can. J. Chem. Eng.* **2015**, *93*, 1793–1801, doi:10.1002/cjce.22272.
21. Zhou, E.; Fan, X.; Dong, L.; Zhao, Y.; Yang, X.; Duan, C.; Liu, Q. Process optimization for arsenic removal of fine coal in vibrated dense medium fluidized bed. *Fuel* **2018**, *212*, 566–575, doi:10.1016/j.fuel.2017.10.085.
22. SSulaiman, S.A.; Miin, C.S.; Naz, M.Y.; Raghavan, V.R. Particle image velocimetry of a swirling fluidized bed at different blade angles. *Chem. Eng. Technol.* **2016**, *39*, 1151–1160, doi:10.1002/ceat.201500074.
23. Li, J.; Yao, X.; Liu, L.; Lu, C. Investigation on distribution of particles in inlet region of an FCC external catalyst cooler with different inlet structures. *Powder Technol.* **2020**, *362*, 267–277, doi:10.1016/j.powtec.2019.11.062.
24. Yao, X.; Zhang, Y.; Lu, C.; Wen, D. CFD investigation of gas-solids flow in a new fluidized catalyst cooler. *Powder Technol.* **2016**, *304*, 108–119, doi:10.1016/j.powtec.2016.08.022.
25. Amiri, Z.; Movahedirad, S.; Shirvani, M. Particles mixing induced by bubbles in a gas-solid fluidized bed. *AIChE J.* **2016**, *62*, 1430–1438, doi:10.1002/aic.15150.
26. Shrestha, S.; Kuang, S.; Yu, A.; Zhou, Z. Particle shape effect on bubble dynamics in central air jet pseudo-2D fluidized beds: A CFD-DEM study. *Chem. Eng. Sci.* **2019**, *201*, 448–466, doi:10.1016/j.ces.2019.02.030.
27. Shrestha, S.; Gan, J.; Zhou, Z. Micromechanical analysis of bubbles formed in fluidized beds operated with a continuous single jet. *Powder Technol.* **2019**, *357*, 398–407, doi:10.1016/j.powtec.2019.08.091.
28. Sarbanha, A.A.; Movahedirad, S.; Ehsani, M. On the hydrodynamics of a pseudo two-dimensional two-zone gas-solid fluidized bed. *Chem. Eng. J.* **2018**, *350*, 971–981, doi:10.1016/j.cej.2018.06.067.
29. Bakshi, A.; Ghoniem, A.F.; Altantzis, C. Mixing dynamics in bubbling fluidized beds. *AIChE J.* **2017**, *63*, 4316–4328, doi:10.1002/aic.15801.

30. Poós, T.; Szabó, V. Volumetric heat transfer coefficient in fluidized-bed dryers. *Chem. Eng. Technol.* **2018**, *41*, 628–636, doi:10.1002/ceat.201700038.
31. Yao, X.; Zhang, Y.; Lu, C.; Han, X. Investigation of the heat transfer intensification mechanism for a new fluidized catalyst cooler. *AIChE J.* **2015**, *61*, 2415–2427, doi:10.1002/aic.14841.
32. Zhang, Y.; Wei, Q. CPFD simulation of bed-to-wall heat transfer in a gas-solids bubbling fluidized bed with an immersed vertical tube. *Chem. Eng. Process. Process Intensif.* **2017**, *116*, 17–28, doi:10.1016/j.cep.2017.03.007.
33. Taofeeq, H.; Al-Dahhan, M. Heat transfer and hydrodynamics in a gas-solid fluidized bed with vertical immersed internals. *Int. J. Heat Mass Transf.* **2018**, *122*, 229–251, doi:10.1016/j.ijheatmasstransfer.2018.01.093.
34. Hofer, G.; Schöny, G.; Pröll, T. Acting on hydrodynamics to improve the local bed-to-wall heat transfer in bubbling fluidized beds. *Chem. Eng. Res. Des.* **2018**, *134*, 309–318, doi:10.1016/j.cherd.2018.04.015.
35. Yang, L.; Zhan, W. New concept for ADS spallation target: Gravity-driven dense granular flow target. *Sci. China Ser. E Technol. Sci.* **2015**, *58*, 1705–1711, doi:10.1007/s11431-015-5894-0.
36. Lytvynenko; Yukhymenko, M.; Pavlenko, I.; Pitel, J.; Mižáková, J.; Ostroha, R.; Bocko, J. Ensuring the reliability of pneumatic classification process for granular material in a rhomb-shaped apparatus. *Appl. Sci.* **2019**, *9*, 1604, doi:10.3390/app9081604.
37. Grbavčić, Ž.B.; Garić-Grulović, R.; Arsenijević, Z.L. Prediction of the choking velocity and voidage in vertical pneumatic conveying of coarse particles. *Powder Technol.* **2006**, *161*, 1–9, doi:10.1016/j.powtec.2005.08.013.
38. Artyukhov, A.; Artyukhova, N.; Ivaniia, A. Creation of software for constructive calculation of devices with active hydrodynamics. In Proceedings of the 2018 14th International Conference on Advanced Trends in Radioelecrtronics, Telecommunications and Computer Engineering (TCSET), Institute of Electrical and Electronics Engineers (IEEE), Slavske, Ukraine, 20–24 February 2018; pp. 139–142.

39. Artyukhov, A.E.; Sklabinskyi, V. Theoretical Analysis of Granules Movement Hydrodynamics in the Vortex Granulators of Ammonium Nitrate and Carbamide Production. *Chem. Chem. Technol.* **2015**, *9*, 175–180, doi:10.23939/chcht09.02.175.
40. Artyukhov, A.; Obodiak, V.; Boiko, P.; Rossi, P. Computer modeling of hydrodynamic and heat-mass transfer processes in the vortex type granulation devices. *CEUR Workshop Proc.* **2017**, *1844*, 33–47.
41. Artyukhov, A.E.; Sklabinskiy, V.I. Investigation of the temperature field of coolant in the installations for obtaining 3D nanostructured porous surface layer on the granules of ammonium nitrate. *J. Nano Electron. Phys.* **2017**, *9*, 1015, doi:10.21272/jnep.9(1).01015.
42. Artyukhov, A.E.; Sklabinskyi, V.I. Experimental and industrial implementation of porous ammonium nitrate producing process in vortex granulators. *Науковий вісник НГУ* **2013**, *6*, 42–48.
43. Yukhymenko, M.; Ostroha, R.O.; Artyukhov, A.E. Hydrodynamic and kinetic processes of the mineral fertilizer granules encapsulating in the multistage device with suspended layer. *East.-Eur. J. Enterp. Technol.* **2016**, *6*, 22–28, doi:10.15587/1729-4061.2016.84179.
44. Yukhymenko, M.; Ostroha, R.; Lytvynenko, A.; Mikhajlovskiy, Y.; Bocko, J. Cooling process intensification for granular mineral fertilizers in a multistage fluidized bed device. *Adv. Manuf. Process.* **2020**, *2*, 249–257, doi:10.1007/978-3-030-50491-5_24.
45. Yukhymenko, M.; Ostroha, R.; Litvinenko, A.; Bocko, J. Estimation of gas flow dustiness in the main pipelines of booster compressor stations. *IOP Conf. Ser. Mater. Sci. Eng.* **2017**, *233*, 012026, doi:10.1088/1757-899x/233/1/012026.
46. Malewski, J. On accuracy of sieve analysis. In Proceedings of the Annual Conference on Aggregates KruszMin'17, Wroclaw, Poland, 10–12 April 2017; pp. 103–111.
47. Retsch GmbH Haan. Sieve analysis. In *Taking a Close Look at Quality*; Retsch GmbH Haan: Haan, Germany, 2009; 52p.

48. Green, D.W.; Southard, Z.M. *Perry's Chemical Engineers' Handbook*, 9th ed.; McGraw Hill Professional: New York, NY, USA, 2018; 2352p.
49. Yukhimenko, N.; Vakal, S. The exergy analysis of energy efficiency of the technology of granulated phosphorus-potassium fertilizers. *East.-Eur. J. Enterp. Technol.* **2016**, *5*, 4–10, doi:10.15587/1729-4061.2016.77182.
50. Luikov, A. *Analytical Heat Diffusion Theory*; Academic Press: New York, NY, USA, 1968; 685p.
51. Wang, S.; Xu, C.; Liu, W.; Liu, Z. Numerical Study on Heat Transfer Performance in Packed Bed. *Energies* **2019**, *12*, 414, doi:10.3390/en12030414.
52. Messai, S.; El Ganaoui, M.; Sghaier, J.; Belghith, A. Experimental study of the convective heat transfer coefficient in a packed bed at low Reynolds numbers. *Therm. Sci.* **2014**, *18*, 443–450, doi:10.2298/tsci120715108m.
53. Schulz, H. *Hydrodynamics—Concepts and Experiments*; InTech: Nappanee, IN, USA, 2015.
54. Moran, S. How to do hydraulic calculations. In *An Applied Guide to Process and Plant Design*; Elsevier: Amsterdam, The Netherlands, 2015; pp. 115–126. (Butterworth-Heinemann is an imprint).
55. Artyukhova, N.; Yuhimenko, M.; Shandyba, O.; Artyukhov, A. Simulation of the particle motion in devices with vertical sectioning of workspace. *Ukr. Food J.* **2014**, *3*, 446–453.
56. Gupta, S.C. *Fluid Mechanics and Hydraulic Machines*; Pearson Education: Karnataka, India, 2006.
57. Yukhymenko, M. *Kinetics of the Heat Exchange and Reduction of the Energy Consumption during the Convection Cooling Process of the Granular Material*; Bulletin Sumy National Agrarian University: Kyiv, Ukraine, 2001; Volume 7, pp. 119–124.
58. Erro, J.; Urrutia, O.; Baigorri, R.; Fuentes, M.; Zamarreño, A.M.; Garcia-Mina, J.M. Incorporation of humic-derived active molecules into compound NPK granulated

fertilizers: main technical difficulties and potential solutions. *Chem. Biol. Technol. Agric.* **2016**, *3*, 2–15, doi:10.1186/s40538-016-0071-7.

59. Lee, R.G.; Kpytowski, J.A. *Fertilizer Manual. United Nations Industrial Development Organization (UNIDO) and International Fertilizer Development Center (IFDC)*; Kluwer Academic Publishers: Dordrecht, The Netherlands, 1998; 615p.
60. Kryukov, G.V.; Tereshchenkov, V.V.; Lykov, M.V.; Gabeskiriya, O.V. Calculations foe single-stage fluidized-bed equipment for cooling mineral fertilizers. *Chem. Pet. Eng.* **1976**, *12*, 141–144, doi:10.1007/bf01144230.
61. Miranda, R.C.; Neto, J.F.G.; Aguiar, B.B.A.; Martins, M.; Silva, C.L.S. Model predictive control of potassium chloride drying by fluidized bed dryer. *IFAC Proc.* **2013**, *46*, 76–80, doi:10.3182/20130825-4-US-2038.00065.
62. Sahoo, P. *Probability and Mathematical Statistics*; University of Louisville: Louisville, KY, USA, 2013; 712p.
63. Shao, J. *Mathematical Statistics*; Springer: New York, NY, USA, 2003; 592p, doi:10.1007/b97553.
64. Rice, J.A. *Mathematical Statistics and Data Analysis*; Thomson Brooks Cole: Duxbury, MA, USA, 2010.
65. Janssen TJ (2011) Explosive Materials: Classification, Composition and Properties. Nova Science Publishers, Inc.
66. Artyukhov A, Obodiak V, Boiko P, Rossi P (2017) Computer modeling of hydrodynamic and heat-mass transfer processes in the vortex type granulation devices. CEUR Workshop Proceedings 1844: 33–47
67. Viktorov SD, Frantov AE, Lapikov IN, Andreev VV, Starshinov AV (2016) Effect of the microstructure of ammonium nitrate granules on the detonability of composite propellants based on it. Combustion, Explosion, and Shock Waves 52(6):727–731.
68. Biessikirski A, Kuterasiński L, Dworzak M, Pyra J, Twardosz M (2019) Comparison of structure, morphology, and topography of fertilizer-based explosives applied in the mining industry. Microchemical Journal 144:39–44.

69. Erode GM (2013) Ammonium Nitrate Explosives for Civil Applications: Slurries, Emulsions and Ammonium Nitrate Fuel Oils. Weinheim: Wiley-VCH Verlag & Co.
70. Artyukhov AE, Sklabinskiy VI (2013) Experimental and industrial implementation of porous ammonium nitrate producing process in vortex granulators. Naukovyi Visnyk Natsionalnoho Hirnychoho Universytetu 6:42–48.
71. Artyukhov A, Artyukhova N, Ivaniia A (2018b) Creation of software for constructive calculation of devices with active hydrodynamics. 14th International Conference on Advanced Trends in Radioelectronics, Telecommunications and Computer Engineering, TCSET 2018 - Proceedings 2018-April: 139–142
72. Artyukhova NO (2020) Morphological features of the nanoporous structure in the ammonium nitrate granules at the final drying stage in multistage devices. Journal of Nano- and Electronic Physics 12(4):04036-1–04036-6.
73. Martin G, Barbour W (2003) Industrial nitrogen compounds and explosives, Chemical Manufacture and Analysis. Watchmaker Publishing.
74. Artyukhov A, Artyukhova N (2018a) Utilization of dust and ammonia from exhaust gases: new solutions for dryers with different types of fluidized bed. Journal of Environmental Health Science and Engineering 16:193–204.
75. Artyukhov AE, Artyukhova NO (2019) Technology and the main technological equipment of the process to obtain N_4HNO_3 with Nanoporous Structure. Springer Proceedings in Physics 221:585-594.
76. Artyukhov A, Artyukhova N, Krmela J, Krmelova V (2020) Complex designing of granulation units with application of computer and software modeling: Case “Vortex granulator”. IOP Conference Series: Materials Science and Engineering 776(1):012016.
77. Pabis S, Jayas DS, Cenkowski S (1998) Grain Drying: Theory and Practice. Wiley
78. Chen XD, Putranto A (2013) Modelling Drying Processes. A Reaction Engineering Approach. Cambridge University Press.
79. Anderson J-O (2014) Energy and Resource Efficiency in Convective Drying Systems in the Process Industry (doctoral thesis). Luleå University of Technology.

80. Wan Daud WR (2008) Fluidized Bed Dryers – Recent Advances. Advanced Powder Technology 19(5):403–418.
81. Kudra T, Mujumdar AS (2002) Advanced Drying Technologies. New York: Marcel Dekker.
82. Barrozo MAS, Mujumdar A, Freire J.T (2014) Air-Drying of Seeds: A Review. Drying Technology, 32:10, 1127-1141
83. Torrecilla JS, Aragon JM, Palancar MC (2006) Improvement of fluidized-bed dryers for drying solid waste (olive pomace) in olive oil mills. European Journal of Lipid Science and Technology 108(11):913-924
84. Alaathar I, Hartge E-U, Heinrich S, Werther J (2013) Modeling and flowsheet simulation of continuous fluidized bed dryers. Powder Technology 238:132–141
85. Kemp IC, Bahu RE (1995) A New Algorithm for Dryer Selection, Drying Technology, 13:5–7.
86. Jittanit W, Srzednicki G, Driscoll RH (2013) Comparison Between Fluidized Bed and Spouted Bed Drying for Seeds. Drying Technology, 31:1.
87. Setty YP, Kumar GV, Srinivas G (2011) Drying of solids in a circulating fluidized bed. The IUP Journal of Chemical Engineering 3(4): 7–16.
88. Motevali A, Minaei S, Banakar A, Ghobadian B, Khoshtaghaza MH (2014) Comparison of energy parameters in various dryers. Energy Conversion and Management 87:711–725
89. Obodiak V, Artyukhova N, Artyukhov A (2020) Calculation of the residence time of dispersed phase in sectioned devices: Theoretical basics and software implementation. Advances in Design, Simulation and Manufacturing II. DSMIE 2019. Lecture Notes in Mechanical Engineering 813–820.
90. Artyukhova NO, Krmela J (2019) Nanoporous structure of the ammonium nitrate granules at the final drying: the effect of the dryer operation mode. Journal of Nano- and Electronic Physics 11(4):04006-1–04006-4.
91. Luikov A (1968) Analytical Heat Diffusion Theory. Academic Press, USA.

92. Faghri A, Zhang Y, Howell J (2010) Advanced Heat and Mass Transfer. Global Digital Press.
93. Van't Land CM (2012) Drying in the Process Industry. John Wiley & Sons, Inc.
94. Dincer I, Zamfirescu C (2016) Drying Phenomena: Theory and Applications. Wiley.
95. Mujumdar AS (2006) Handbook of Industrial Drying. Boca Raton: Taylor & Francis Group.
96. Yukhymenko M, Ostroha R, Artyukhov A, Bocko J (2020) Effect of Temperature on Formation of Nanoporous Structure of Granule Shell in Technology of Obtaining Organo-mineral Fertilizers. Nanooptics and Photonics, Nanochemistry and Nanobiotechnology, and Their Applications. Springer Proceedings in Physics 247:159–169.
97. Sazhin B, Sazhin V (2007) Scientific Principles of Drying Technology. New York – Connecticut – Wallingford (U.K.): Begell House Inc.
98. Artyukhov A, Artyukhova N 2018 *Journal of Environmental Health Science and Engineering* **16** 193–204.
99. Artyukhova N O, Krmela J 2019 *Journal of Nano- and Electronic Physics* **11(4)** 04006-1-04006-4.
100. Gidaspow D 1994 *Multiphase flow and fluidization: continuum and kinetic theory descriptions with applications* (Academic Press, San Diego).
101. Yang W C 2003 *Handbook of fluidizfition and fluid-particle systems* (Marcel Dekker, New York).
102. Gibilaro L G 2001 *Fluidization-dynamics. The formulation and applications of a predictive theory for the fluidized state* (Butterworth-Heinemann, Woburn).
103. Pabis S, Jayas D S, Cenkowski S 1998 *Grain Drying: Theory and Practice* (Wiley).
104. Artyukhova N.O. 2018 Journal *of Nano- and Electronic Physics* **10(3)** 03030.
105. Artyukhov A, Artyukhova N, Ivaniia A, Gabrusenoks J 2017 *IEEE International Young Scientists Forum on Applied Physics and Engineering (YSF-2017)* 315-318.
106. Artyukhov A, Artyukhova N, Krmela J, Krmelova V 2020 *IOP Conference Series: Materials Science and Engineering* **776(1)** 012016.

107. Krmela J, Artyukhova N, Artyukhov A 2020 *Manufacturing Technology* **20(4)** 468-473.
108. Patent 74070 Ukraine *Device for drying of disperse materials*.
109. Patent 81720 Ukraine *Device for drying of disperse materials*.
110. Patent 92423 Ukraine *Device for drying of disperse materials*.
111. M. Kwauk, *Fluidization: Idealized and bubbleless, with application*, Science Press, Beijing, 1992.
112. D. Gidaspow, *Multiphase flow and fluidization: continuum and kinetic theory descriptions with applications*, Academic Press, San Diego, 1994.
113. W.-C. Yang, *Handbook of fluidizfition and fluid-particle systems*, Marcel Dekker, New York, 2003.
114. L.G. Gibilaro, *Fluidization-dynamics. The formulation and applications of a predictive theory for the fluidized state*, Butterworth-Heinemann, Woburn, 2001.
115. P. Muralidhar, E.Bhargav and C. Sowmya, "Novel techniques of granulation: a review", International Research Journal of Pharmacy 7(10), 8–13 (2016).
116. H. Stahl, "Comparing Different Granulation Techniques", Pharmaceutical Technology Europe, 23–33 (2004).
117. D. Parikh, *Handbook of Pharmaceutical Granulation Technology*, Informa Healthcare, 2009.
118. H. Stahl, Comparing Granulation Method, Hürth: GEA Pharma Systems, 2010.
119. H. K. Solanki, T. Basuri, J.H. Thakkar and C.A. Patel, "Recent advances in granulation technology" International Journal of Pharmaceutical Sciences Review and Research 5(3), 48–54 (2010).
120. S. Srinivasan, "Granulation techniques and technologies: recent progresses", Bioimpacts 5(1), 55–63 (2015).
121. M.A. Saikh, "A technical note on granulation technology: a way to optimise granules", International Journal of Pharmaceutical Sciences Review and Research 4, 55–67 (2013).

122. P. Patel, D. Telange and N. Sharma, “Comparison of Different Granulation Techniques for Lactose Monohydrate”, International Journal of Pharmaceutical Sciences and Drug Research 3, 222–225 (2011).
123. V.A. Kirsanov and M.V. Kirsanov, Effect of Structural Parameters of Cascade Elements on Effectiveness of Pneumatic Classification”, Chemical and Petroleum Engineering 49, 707–711 (2014).
124. V.A. Kirsanov and M.V. Kirsanov, “Hydrodynamic Characteristics of Classification Process in Pneumatic Classifier with Continuous Shelves”, Chemical and Petroleum Engineering 54, 71–74 (2018).
125. M. Yukhymenko, R.Ostroha, A. Lytvynenko, Y. Mikhajlovskiy and J.Bocko, “Cooling Process Intensification for Granular Mineral Fertilizers in a Multistage Fluidized Bed Device”, Lecture Notes in Mechanical Engineering, 249–257 (2020).
126. M. Yukhymenko and A. Lytvynenko, “Pneumatic Classification Of The Granular Materials In The “Rhombic”Apparatus”, Journal of Manufacturing and Industrial Engineering 1-2, 1–3 (2014).
127. E. Barsky and M. Barsky, “Master curve of separation processes”, Physical Separation in Science and Engineering 13(1), 1–13 (2004).
128. E. Barsky and M. Barsky. *Cascade Separation of Powders*, Cambridge Int Science Publishing, 2006.
129. A.E. Artyukhov, V.K. Obodiak, P.G. Boiko and P.C. Rossi, “Computer modeling of hydrodynamic and heat-mass transfer processes in the vortex type granulation devices”, in *CEUR Workshop Proceedings* 1844, pp. 33-47, 2017.
130. A.E. Artyukhov, N.A. Artyukhova, „Utilization of dust and ammonia from exhaust gases: new solutions for dryers with different types of fluidized bed”, *Journal of Environmental Health Science and Engineering* 16 (2), 193-204 (2018).
131. A. Artyukhov, N.Artyukhova, A. Ivaniia, R. Galenin, “Progressive equipment for generation of the porous ammonium nitrate with 3D nanostructure”, *Proceedings of the 2017 IEEE 7th International Conference on Nanomaterials: Applications and Properties*, NAP 2017, 03NE06 (2017).

132. A. Artyukhov , N. Artyukhova , J. Krmela , V. Krmelova, "Complex designing of granulation units with application of computer and software modeling: Case "Vortex granulator". *IOP Conference Series: Materials Science and Engineering* 776(1), 012016 (2020).

133. N.A. Artyukhova, "Multistage finish drying of the N_4HNO_3 porous granules as a factor for nanoporous structure quality improvement", Journal of Nano- and Electronic Physics 10 (3), 03030-1–03030-5 (2018).

134. A.E. Artyukhov, N.O. Artyukhova and A.V. Ivaniia, "Creation of software for constructive calculation of devices with active hydrodynamics", in Proceedings of the 14th International Conference on Advanced Trends in Radioelectronics, Telecommunications and Computer Engineering (TCSET 2018), pp. 139-142, 2018.

135. A.E. Artyukhov, N.A. Artyukhova, A.V. Ivaniia and J. Gabrusenoks, "Multilayer modified NH_4NO_3 granules with 3D nanoporous structure: effect of the heat treatment regime on the structure of macro- and mezopores", in Proc IEEE International Young Scientists Forum on Applied Physics and Engineering (YSF-2017), pp. 315–318 (2017).

136. A.E. Artyukhov, V.I. Sklabinskiy, "Application of vortex three-phase separators for improving the reliability of pump and compressor stations of hydrocarbon processing plants", IOP *Conference Series: Materials Science and Engineering*, 233(1), 012014 (2017).

137. K. Hiltunen, A. Jasberg, S. Kallio, H. Karema, M. Kataja, A. Koponen, M. Manninen and V. Taivassalo, *Multiphase Flow Dynamics: Theory and Numerics*, VTT Technical Research Centre of Finland, Edita Prima Oy, 2009.

138. C. Crowe, *Multiphase flow handbook*, Boca Raton, Taylor & Francis Group, 2006.

139. D.L. Marchisio, R.O. Fox, *Computational Models for Polydisperse Particulate and Multiphase Systems*. Cambridge Series in Chemical Engineering. Cambridge University Press, 2013.

140. D. Gidaspow, *Multiphase flow and fluidization: continuum and kinetic theory descriptions with applications,* Academic Press, San Diego, 1994.

141. E.G. Sinaiski, *Hydromechanics: theory and fundamentals*. Weinheim, WILEY-VCH Verlag GmbH & Co. KGaA, 2010.

142. A.E. Artyukhov and N.O. Artyukhova, "Technology and the main technological equipment of the process to obtain NH_4NO_3 with nanoporous structure", *Springer Proceedings in Physics* 221, 585–594 (2019).

143. K.P. Bowman, J.C. Lin, A. Stohl, R. Draxler, P. Konopka, A. Andrews and D. Brunner, "Input Data Requirements for Lagrangian Trajectory Models", Bulletin *of the American Meteorological Society* 94, 1051-1058 (2013).

144. M. Rybalko, E. Loth and D. Lankford, "A Lagrangian particle random walk model for hybrid RANS/LES turbulent flows", *Powder Technology* 221, 105-113 (2012).

145. A. I. Leont'ev, Kuzma-Kichta, Yu. A., Popov I. A.: "Heat and mass transfer and hydrodynamics in swirling flows (review)", *Thermal Engineering* 64 (2), 111-126 (2017).

146. M. Honkanen, *Direct optical measurement of fluid dynamics and dispersed phase morphology in multiphase flows. Thesis for the degree of Doctor of Technology*, Tampere Univetsity of Technology, 193 p., 2006.

147. M.J.V. Goldschmidt, G.G.C. Weijers, R. Boerefijn and J.A.M. Kuipers, „Discrete element modelling of fluidised bed spray granulation", *Powder Technology* 138, 39-45 (2003).

148. M. Khanali, S. Rafiee, A. Jafari and A. Banisharif, "Study of Residence Time Distribution of Rough Rice in a Plug Flow Fluid Bed Dryer", *International Journal of Advanced Science and Technology* 48, 103-114 (2012).

149. S. Banerjee, R.K. Agarwal, "Review of recent advances in process modeling and computational fluid dynamics simulation of chemical-looping combustion", *International Journal of Energy for a Clean Environment* 18 (1), 1-37 (2018).

150. Certificate of copyright registration No. 79141UA, UA: Computer program "Multistage fluidizer" (2018).

151. A. Artyukhov, N. Artyukhova, R. Ostroha, M. Yukhymenko, J. Bocko and J. Krmela. Convective drying in the multistage shelf dryers: theoretical bases and practical implementation, *Drying Unit Operations*. – IntechOpen, UK, 140-163 (2019).

152. B. Paprocki, A. Pregowska and J. Szczepanski, “Optimizing information processing in brain-inspired neural networks”, *Bull. Pol. Ac.: Tech*. 68 (2), 225-233 (2020). DOI: 10.24425/bpasts.2020.131844

153. W. Jefimowski, A. Nikitenko, Z. Drążek and M. Wieczorek, “Stationary supercapacitor energy storage operation algorithm based on neural network learning system”, *Bull. Pol. Ac.: Tech*. 68 (4), 733-738 (2020). DOI: 10.24425/bpasts.2020.134176